Modeling fast-ion transport during toroidal Alfvén eigenmode avalanches in National Spherical Torus Experiment

E. D. Fredrickson,[1,a)] N. A. Crocker,[2] R. E. Bell,[1] D. S. Darrow,[1] N. N. Gorelenkov,[1] G. J. Kramer,[1] S. Kubota,[2] F. M. Levinton,[3] D. Liu,[4] S. S. Medley,[1] M. Podestá,[4] K. Tritz,[5] R. B. White,[1] and H. Yuh[3]
[1]*Princeton Plasma Physics Laboratory, Princeton, New Jersey 08543, USA*
[2]*University of California, Los Angeles, California 90095, USA*
[3]*Nova Photonics, Princeton, New Jersey 08543, USA*
[4]*University of California, Irvine, California 92697, USA*
[5]*Johns Hopkins University, Baltimore, Maryland 21287, USA*

(Received 20 August 2009; accepted 23 October 2009; published online 9 December 2009)

Experiments on the National Spherical Torus Experiment [M. Ono *et al.*, Nucl. Fusion **40**, 557 (2000)] found strong bursts of toroidal Alfvén eigenmode (TAE) activity correlated with abrupt drops in the neutron rate. A fairly complete data set offers the opportunity to benchmark the NOVA [C. Z. Cheng, Phys. Rep. **211**, 1 (1992)] and ORBIT [R. B. White and M. S. Chance, Phys. Fluids **27**, 2455 (1984)] codes in the low aspect ratio tokamak (ST) geometry. The internal structure of TAE was modeled with NOVA and good agreement is found with measurements made with an array of five fixed-frequency reflectometers. The fast-ion transport resulting from these bursts of multiple TAE was then modeled with the ORBIT code. The simulations are reasonably consistent with the observed drop in neutron rate, however, further refinements in both the simulation of the TAE structure and in the modeling of the fast-ion transport are needed. Benchmarking stability codes against present experiments is an important step in developing the predictive capability needed to plan future experiments. © *2009 American Institute of Physics*. [doi:10.1063/1.3265965]

I. INTRODUCTION

A broad spectrum of instabilities[1] is found to be excited in the National Spherical Torus Experiment (NSTX) (Ref. 2) during heating by neutral beam injection (NBI). The neutral beams can be injected with energies between 60 and 95 kV. The beam ion velocities (at full energy) are typically several times faster than the Alfvén speed, V_A in the plasma. Two classes of these beam driven instabilities are correlated with significant drops in the neutron rate (losses of fast ions);[3–19] a strongly chirping, fishbonelike energetic particle mode (EPM)[20–35] and strong bursts of multiple, frequency chirping, toroidal Alfvén eigenmodes (TAEs).[36–94] The TAE bursts are believed to be an example of the synergistic interaction of multiple modes causing nonlinear enhancement in fast ion transport, that is TAE avalanches.[95–97] Individual TAEs are considered unlikely to cause significant fast-ion losses in ITER,[94] but the interaction of multiple TAE is considered a possible concern for enhanced transport of the fusion α's in ITER.[97]

In this paper we will describe an experiment to identify the threshold for excitation of TAE and the TAE bursts and to acquire data needed to benchmark the ideal stability code, NOVA,[98,99] and the particle tracking code, ORBIT.[100] Similar analyses of experimental data have been done in the past with varying levels of agreement (cf. Refs. 10, 14, 18, 92, and 93). This paper describes the results from the initial experiments; further experiments with more complete diagnostics will be carried out in coming years. In Sec. II the conditions under which the modes are seen and the diagnostic measurements of the modes and equilibrium are described. Section III describes the reconstruction of the equilibrium and calculation of the fast-ion distribution. In Sec. IV the measurements of the mode structure are compared with the NOVA simulations and Sec. V describes the simulations of the fast-ion transport and loss.

II. EXPERIMENTAL CONDITIONS

The target plasma has a "flat-top" plasma current of 800 kA [Fig. 1(d)] with a nominal toroidal field of 4.5 kG. Neutral beams were used to heat the plasma during the current ramp and to provide a measurement of the initial q-profile with the motional Stark effect (MSE) diagnostic[101] [Figs. 1(b) and 1(c)]. At the current flat-top time ($\approx$0.175 s), the beam power was reduced below the threshold needed to excite TAE activity by substituting a neutral beam source at 70 kV for the 90 kV source used during the current ramp. The fast-ion population built up during the current ramp was then allowed to relax for 65 ms. At 0.24 s an additional source at 65 kV was added to increase the fast-ion beta above the threshold for exciting TAE. TAE onset shortly before 0.25 s and the first strong TAE burst occurs at $\approx$0.258 s [Fig. 1(a)] causing a transient drop in the neutron rate [Fig. 1(c), black curve]. As will be described below, the q-profile is still strongly evolving, reaching $q_{min} \approx 1$ around 0.3 s, at which time a fishbonelike EPM triggered a core kink mode, suppressing the TAE activity, possibly through redistribution of core fast ions. At 0.3 s the 90 kV

a)Author to whom correspondence should be addressed. Electronic mail: efredrickson@pppl.gov.

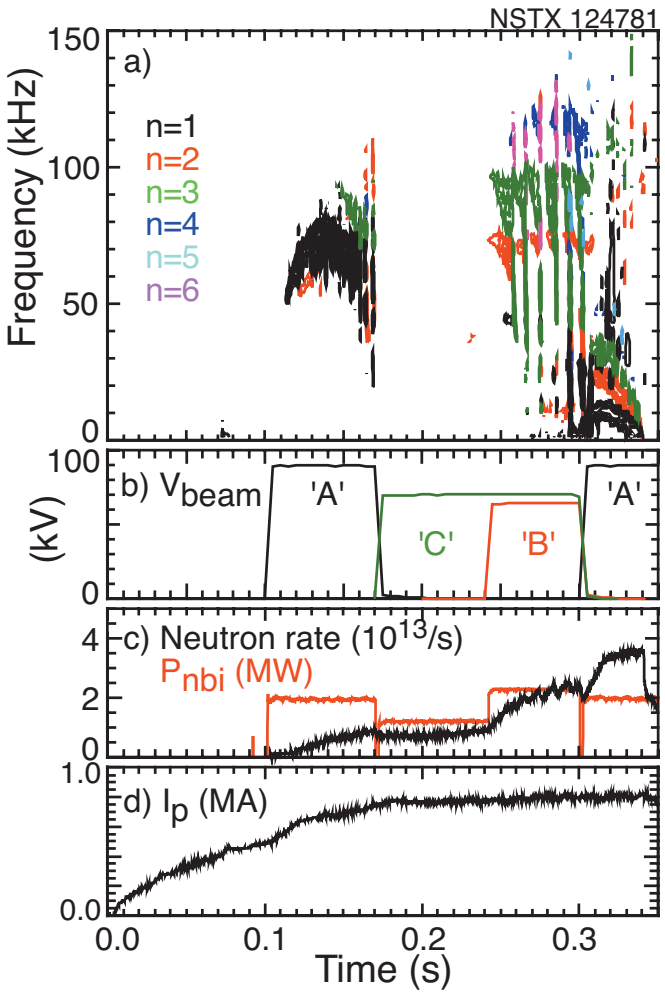

FIG. 1. (Color) (a) Spectrogram of Mirnov coil [black-1, red-2, green-3, blue-4, cyan-5, magenta-6]. (b) Voltage for neutral beam sources "A," "B," and "C." (c) Neutron rate (black) and total injected beam power (red). (d) Plasma current.

source was substituted for the two lower voltage sources to again provide a measurement of the q-profile.

Shown in Figs. 1(b)–1(d) are the time history of the accelerating voltage for each source, the evolution of the plasma current, and the net neutral beam injected power. The beam voltage indicated by the black curve is for source A, the source kept at an accelerating voltage of 90 kV for the MSE diagnostic. Thus, for this shot, the MSE measurements are available from roughly 0.1 to 0.17 s and after 0.3 s. The evolution of the q-profile was measured in a similar shot with source A on from 0.1 to 0.17 s and from 0.24 to 0.46 s. While the bursting character of the modes changed for this slightly lower power (2 MW versus 2.2 MW) and higher beam voltage shot, the q-profiles are found to be in good agreement at 0.32 s suggesting that the current profile evolution is not strongly influenced by the change in beam voltage.

The plasma was kept in L-mode by using a helium prefill and helium gas puffing. The high recycling rate of helium raises the H-mode power threshold. The best diagnostic on NSTX for internal measurements of the evolution of the mode structure and amplitudes is the five-channel reflectometer array, with the highest frequency channel at 50 GHz, or an "O"-mode cutoff density of $\approx 3.1 \times 10^{19}/\mathrm{m}^3$. Thus useful data on the internal mode structure require a peaked (L-mode) density profile with a density on axis between 3.2×10^{19} and $4 \times 10^{19}/\mathrm{m}^3$. The H-mode pedestal density in NSTX H-mode plasmas is typically above the cutoff frequency of the reflectometers and the density profile is often flat in the core region.

Scans of the beam voltage (and thus power) were done with single sources at tangency radii of 49.7 and 59.2 cm from 65 kV ($\approx$1 MW) up to 95 kV ($\approx$2.1 MW) to find the optimum conditions for TAE avalanching. It was found that the most reliable production of TAE avalanches for these L-mode plasmas was by using two lower voltage (65 or 70 kV) beam sources rather than a single higher voltage source at similar power. Two sources at 65 kV (R_{tan}=49.7 and 59.2 cm) are sufficient to excite TAE, and with only slightly more power (an increase in the voltage in one source from 65 to 70 kV), TAE avalanches are seen. These scans were duplicated at higher, 5.5 kG, and lower, 3.5 kG, toroidal field (with same plasma current and nominally the same density). TAE avalanches are more difficult to obtain at low field and marginally easier at higher field, consistent with an interpretation that too large a ratio of V_{fast} to $V_{Alfvén}$ reduces TAE fast-ion drive, presumably by moving the fast ions further above the resonance condition.

Plasma parameters were measured with an array of diagnostics, notably Thomson scattering[102] for electron density and electron temperature profiles [Figs. 2(a) and 2(b)], charge-exchange recombination spectroscopy[103] for ion temperature, toroidal rotation [Fig. 2(c)] and carbon density (the dominant impurity for Z_{eff}) profiles, and MSE for magnetic field pitch angle profiles to constrain equilibrium reconstructions. The MSE diagnostic requires neutral beam source A (tangency radius 69.2 cm) at 90 kV, so experiments were designed to take MSE measurements before and after the time of interest. Similar shots were taken with MSE measurements at the time of interest by substituting the 90 kV, 2 MW source A for the 2.2 MW from the two lower voltage (65 kV/70 kV) sources. Concerns that the change in sources and TAE activity might affect the current profile evolution are somewhat alleviated by comparison of the q-profiles after 300 ms, which find no significant difference.

As mentioned above, L-mode profiles are required to optimize use of the multichannel reflectometer array. For the best radial coverage, the peak density should be in the range from 3.2×10^{19} to $4 \times 10^{19}/\mathrm{m}^3$, and the density profiles should be peaked, that is, L-mode profile shapes. To ensure that the plasma remained in L-mode, plasmas were fueled with Helium from the gas injection system, although the neutral beams continued to operate with deuterium. Thus, there is some uncertainty in the exact composition of the plasma. As will be discussed below, the evolution of the neutron rate in simulations is matched to the measured neutron rate by adjusting the helium to deuterium recycling fractions.

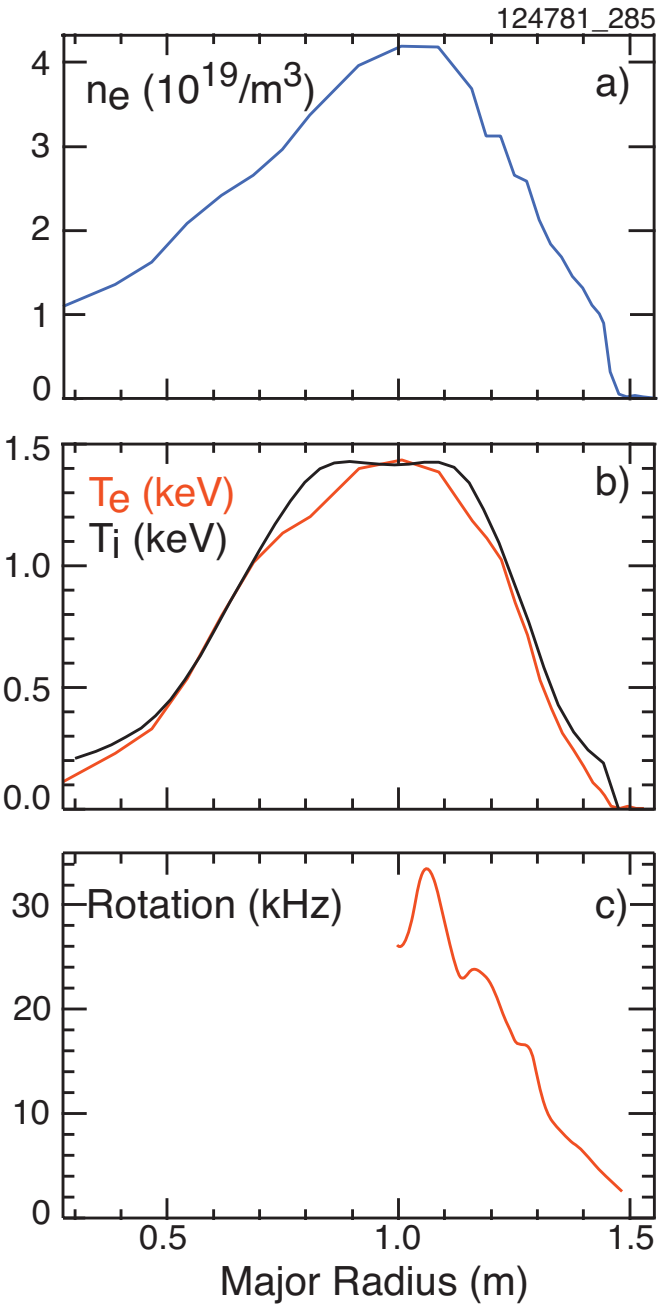

FIG. 2. (Color) (a) Electron density profile. (b) Electron (red) and ion (black) temperature profiles. (c) Rotation profile at 0.285 s for shot shown in Fig. 1.

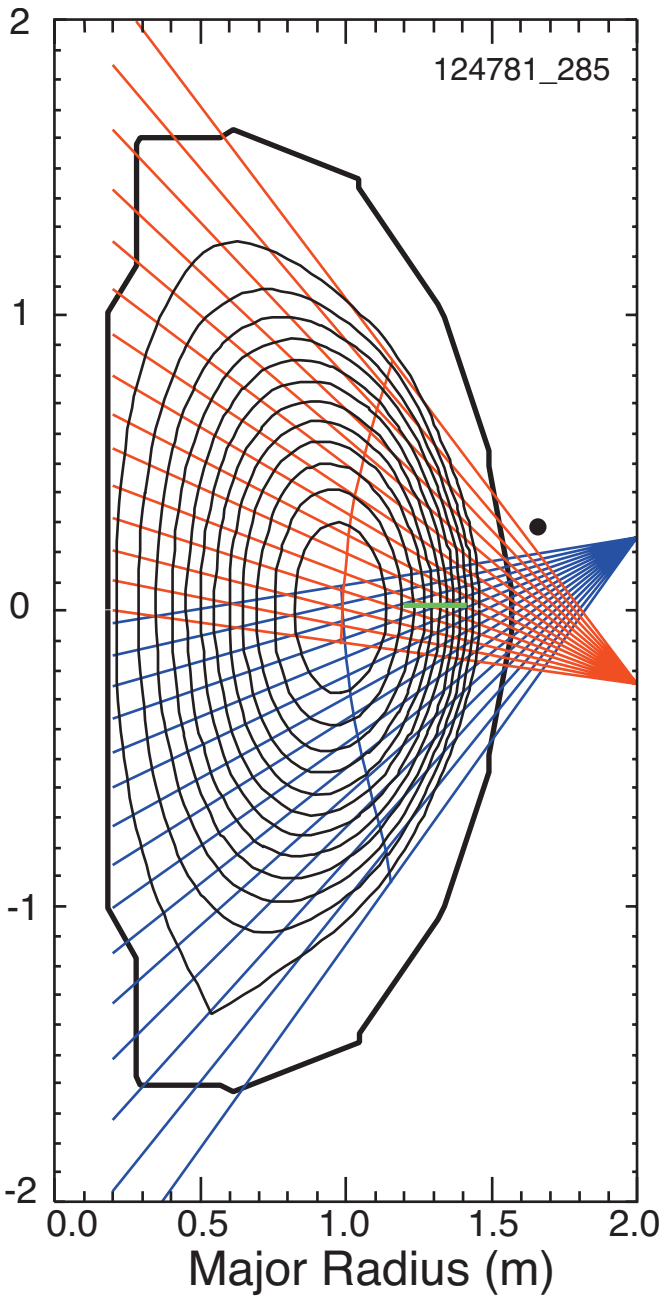

FIG. 3. (Color) Cross section of NSTX showing locations of soft x-ray camera chords (red and blue), range of reflectometer array measurements (green bar), and toroidal arrays of Mirnov coils (black squares). Blue and red arcs are tangency radii for soft x-ray chords. Solid black curve is poloidal projection of limiter surfaces.

A. External and internal measurements of mode structure and amplitude

Diagnostics with the bandwidth and sensitivity to detect TAE modes on NSTX include the arrays of Mirnov coils, reflectometer arrays, interferometer arrays, and soft x-ray cameras.[104] Data used in the analysis of these experiments are primarily from the Mirnov coils and the reflectometer array. The locations of the soft x-ray chords, range of reflectometer measurements, and poloidal location of Mirnov toroidal arrays are shown in Fig. 3.

The primary diagnostics for detection of instabilities in the NSTX plasma are arrays of external magnetic pick-up loops, Mirnov coils. External arrays of Mirnov coils are used to measure the frequency spectrum and toroidal wavelengths of the individual TAE instabilities. In Fig. 1(a), and Fig. 4(a) in more detail, are overlaid spectrograms of the even-n and odd-n magnetic fluctuations. The colors indicate the toroidal mode numbers according to the code: black: n=1, red: n=2, green: n=3, blue: n=4, cyan: n=5, and magenta: n=6. The spectrogram covers the time range from 0.25 to 0.3 s, roughly from the onset of TAE activity until the onset of fishbone modes (when q_{min} drops to near one). The dominant TAE has an onset frequency of ≈100 kHz and toroidal mode number of n=3.

Five strong TAE bursting events are seen in Fig. 4; we

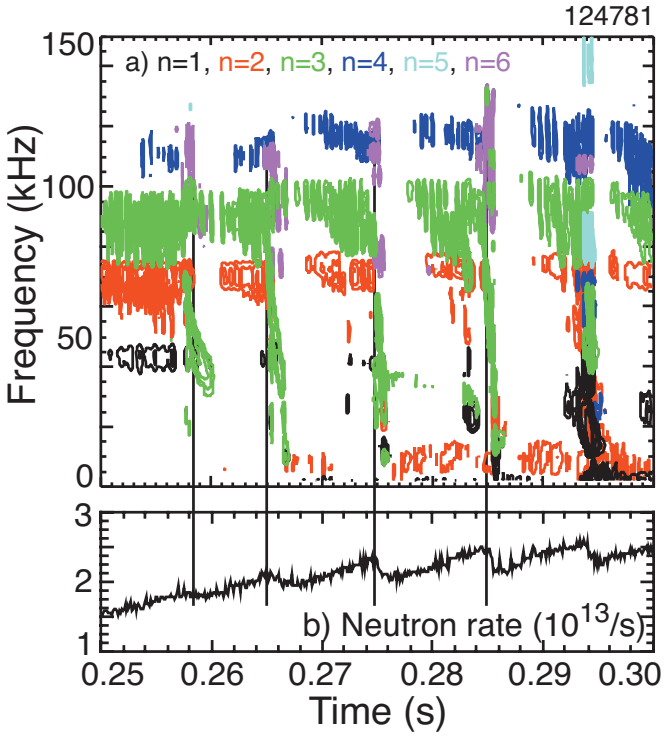

FIG. 4. (Color) (a) Spectrogram of magnetic fluctuations showing sequence of avalanche events; colors indicate toroidal mode numbers [black-1, red-2, green-3, blue-4, cyan-5, magenta-6]. (b) Neutron rate showing drops of ≈10% at avalanches.

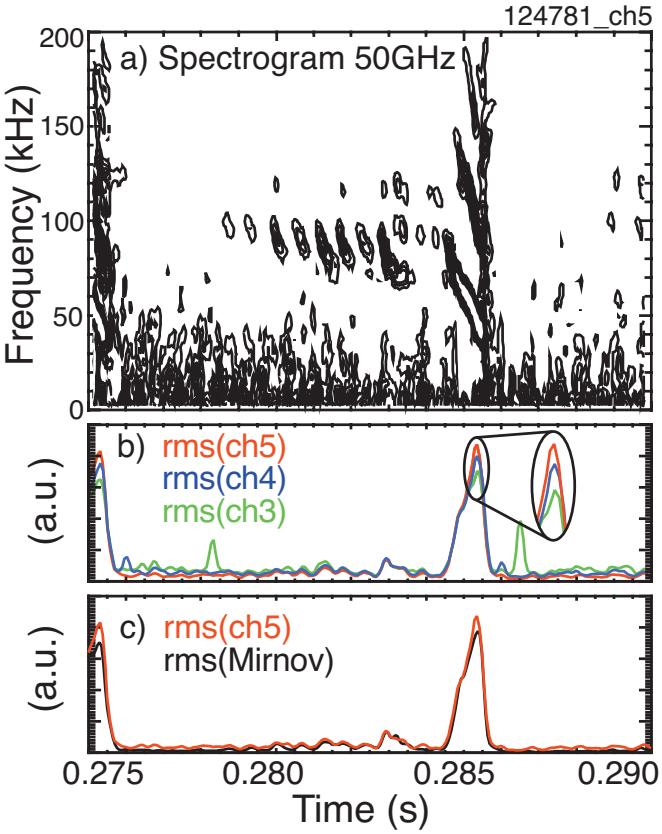

FIG. 5. (Color) (a) Spectrogram of 50 GHz interferometer. (b) rms fluctuation level from 30 to 200 kHz of 50 GHz (red), 42 GHz (blue), and 30 GHz (green) reflectometers. (c) rms fluctuation level from 30 to 200 kHz for Mirnov coil (black) and 50 GHz reflectometer (red).

will consider the possibility that these bursts are TAE avalanches. With each burst, the total TAE amplitude increases by roughly an order of magnitude, the dominant modes show strong downward frequency chirps and there is a drop in the volume neutron emission rate [Fig. 4(b)]. Following each burst, the TAE is quiescent for a short period. The final burst is accompanied by a strong n=1 fishbone mode, indicating a coupling of TAE and fishbone EPMs.

Internal measurements of the TAE amplitude and structure were made with the five fixed-frequency heterodyne and quadrature reflectometers operating in L-mode. The frequencies for the reflectometers are 30, 35, 42, 44.5, and 50 GHz, corresponding to electron density at the cutoff layers of 1.12, 1.52, 2.19, 2.46, and $3.1\times10^{19}/\mathrm{m}^3$, respectively. The peak density, on axis, for the shot discussed here is $4.2\times10^{19}/\mathrm{m}^3$, somewhat higher than optimum. The density cutoff for the highest frequency channel is at a major radius of ≈1.2 m, or just inside the radius of the minimum in q.

A spectrogram of the phase measured by the deepest (50 GHz) channel is shown in Fig. 5(a) for one TAE avalanche sequence. While the amplitude of each mode can be tracked individually, as an example the total rms fluctuation amplitude over the frequency range from 30 to 105 kHz is shown in Fig. 5(b) for the three deepest channels: red −30 GHz, blue −44.5 GHz, and green −42 GHz. This frequency range encompasses both the n=2 and n=3 modes, so does not strictly represent the structure of a single mode. The amplitudes for these three channels are normalized and overlaid to illustrate how well they track each other in time, suggesting that the structure of the modes does not change significantly as the modes grow; except just toward the end. The deepest channel (closest to the magnetic axis) grows relatively faster than the others, suggesting that in the very nonlinear state the mode amplitude becomes slightly more peaked in radius. In Fig. 5(c) is shown a similar figure comparing again the relative amplitude of deepest channel to the magnetic fluctuation amplitude measured at the plasma edge with a Mirnov coil. Again, the amplitudes track well, except at the very largest amplitudes.

The soft x-ray cameras measure the mode fluctuations deeper in the core than the reflectometers. However, due to the complicated structure of the TAE and the chord-integrated nature of soft x-ray data, quantitative comparisons with NOVA simulations are too difficult to be included here. The chord-integrated soft x-ray profiles, the inverted, local soft x-ray emissivity and fluctuation amplitude of the chord integrated emissivity are shown in Fig. 6. Qualitatively, the soft x-ray emissivity is strongly peaked, which implies that much of the fluctuation amplitude seen on the deeper chords originates near the axis, beyond the last reflectometer measurement. (The data shown here are from the avalanche at 0.275 s as some channels were saturated at 0.285 s.)

The Mirnov coil arrays on NSTX include coils oriented to measure the magnetic fluctuations in the toroidal direction, as well as the more standard poloidal orientation. The polarity of the magnetic fluctuations in the poloidal-toroidal plane is measured with this array. In Fig. 7 are shown data from a

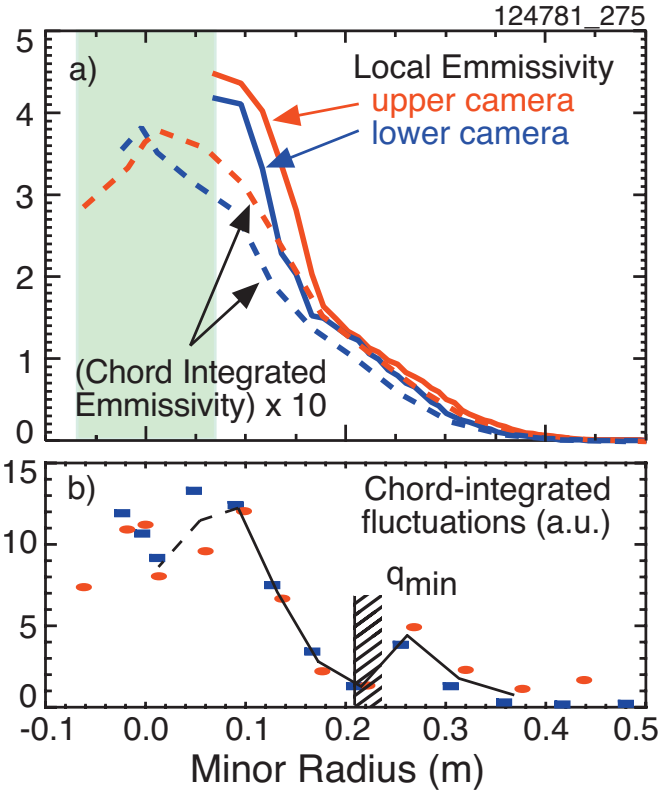

FIG. 6. (Color) (a) Local soft x-ray emissivity (solid lines) and chord integrated (dashed lines) profiles. (b) Chord integrated soft x-ray fluctuations for n=3 mode (red-upper camera, blue-lower camera).

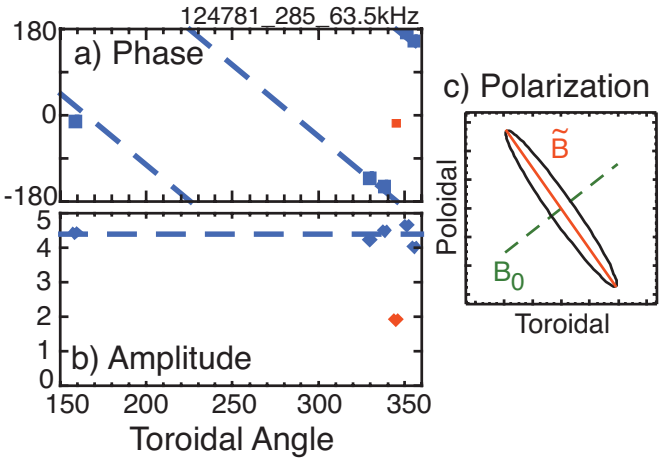

FIG. 7. (Color) Polarization measurement of edge magnetic fluctuations. (a) Relative phase of toroidal Mirnov coil array (blue squares), Mirnov coil oriented to measure toroidal fluctuations (red circle). (b) Amplitudes of magnetic fluctuations. (c) Lissajous figure showing polarization of magnetic fluctuations.

six-coil array. The blue points in Fig. 7 show the relative phases and the amplitudes of the signals from coils oriented to measure the poloidal component of the magnetic fluctuations, the red points show the phase and amplitude from a coil oriented to measure the toroidal component of the magnetic fluctuations. The dashed blue line shows a fit showing that these fluctuations have a toroidal mode number n=3. In Fig. 7(c) is shown a Lissajous pattern created from the average poloidal phase and amplitude data and the phase and amplitude from the toroidally oriented coil compared with the pitch of the equilibrium field (green) at the plasma edge. As TAEs, and most low frequency instabilities, are primarily shear-type modes, the magnetic fluctuations would be expected to be nearly perpendicular to the equilibrium magnetic field. The measured pitch of the magnetic fluctuations, as measured near the vacuum vessel wall, is nearly perpendicular to the equilibrium field at the plasma edge. These measurements will be compared to the polarization of the eigenmodes calculated with the NOVA code in Sec. IV.

B. Measurement of fast-ion redistribution and losses

Diagnostics for the study of fast-ion loss or redistribution on NSTX include the multichannel neutral particle analyzer (NPA) diagnostics, fast neutron rate monitors, and the scintillator-based fast lost ion probe (sFLIP). NSTX has two NPA systems, the first being an "E‖B" system that can be scanned (on a shot-to-shot basis) in tangency radius (from looking co-nbi to ctr-nbi) as well as vertically, with high energy resolution.[105] The second is a fixed four-channel solid-state system with tangency radii of 60, 90, 100, and 120 cm.[106] The sFLIP detector is located on the outboard vacuum vessel wall at a major radius of 1.6 m, 0.14 m below the midplane[107] and measures the pitch and energy of the lost fast ions.

The drops in the neutron rate described above suggest losses of fast ions; an interpretation supported by bursts in edge $D_<$ emission coincident with the neutron drops. The lost fast ions deposit energy on the limiter tiles, increasing the edge recycling. For the events described here, there is no measurable change in the sFLIP signal, indicating that the fast ions were lost to a different area of the vacuum vessel.

In Fig. 8 is shown the energy resolved, time-dependent NPA spectrum at 60 cm tangency radius during the TAE avalanches. Bursts of signal, indicating redistribution of fast-ions, are seen at the time of each avalanche. As the NPA signal quickly returns to its preavalanche level, the data suggest that the fast ions are moving through the instruments sightline. Of particular interest is that the redistribution extends down to energies at least as low as 30 keV, less than half the full energy of injection; this observation is qualitatively consistent with simulations described below. The time resolution and sensitivity are not sufficient to study possible variations in lost-ion energy during the frequency chirp in the final burst.

III. EQUILIBRIUM AND TRANSP ANALYSIS OF THE PLASMA

The plasma equilibrium was reconstructed from magnetics and kinetic data with the LRDFIT equilibrium code. The reconstruction is constrained by the standard flux-loop data, poloidal magnetic field data, and MSE measurements of the magnetic field pitch-angle profile. The reconstruction is further constrained by the full major radial profiles of electron temperature with the assumption of constant electron temperature on a flux surface ("T_e isosurface" constraint).

The reconstructed equilibria form the basis for the TRANSP (Ref. 108) transport analysis. Of particular interest,

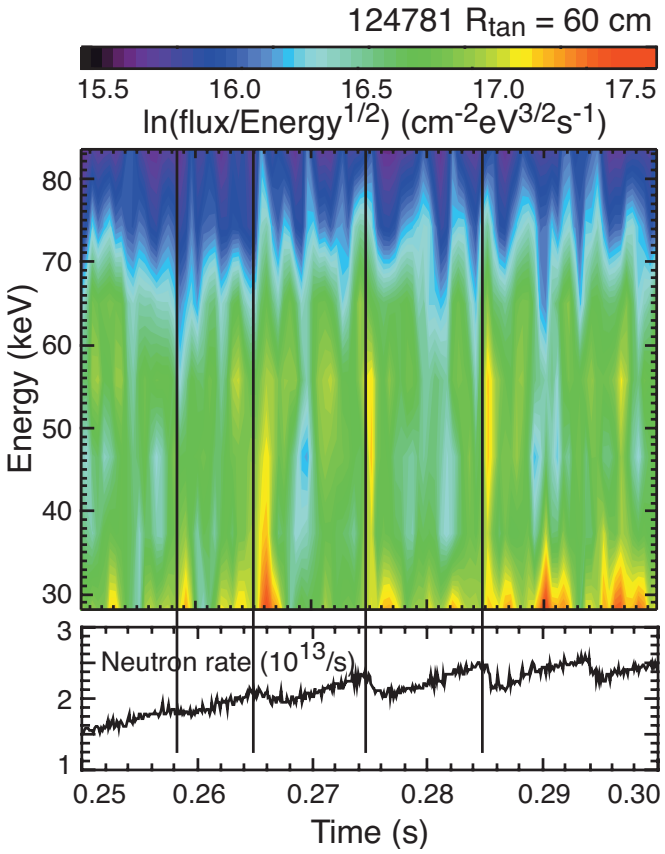

FIG. 8. (Color) Energy spectrum of fast ions from tangentially viewing NPA and neutron rate showing drops of ≈10% at avalanches.

the beam deposition model in TRANSP was used to predict the fast-ion distribution functions which were used as input to the NOVA-K and ORBIT codes. The target plasma is nominally helium, which affects the ratio of beam-target to beam-beam neutron production. The beam-target neutron rate will be roughly linearly proportional to fast-ion density; the beam-beam rate will be approximately quadratic. The helium-deuterium ratio was not independently measured, and thus must be adjusted to fit the evolution of the measured neutron rate. A good fit to the neutron rate evolution was found by modeling the plasma composition as initially helium which is diluted with D recycling from the walls during the shot, and the D-fueling from NBI heating (Fig. 9). The neutron rate evolution in this shot was fit by assuming a constant 13% of the recycled gas from the walls is deuterium, with the rest being helium and trace hydrogen. The TRANSP simulation finds that the neutrons in this "helium plasma" are ≈60% beam-beam and 40% beam-target. Reducing the deuterium recycling fraction to 9% results in ≈70% beam-beam neutrons, ≈30% beam-target. Increasing the deuterium recycling fraction to 20% changes the ratio to ≈55% beam-beam and ≈45% beam-target, but in both cases the predicted neutron rates no longer match the measured neutron rates. If TAEs were causing anomalous fast-ion losses (not modeled in TRANSP), a higher D-recycling fraction would be needed to match the measured neutron rate.

The fast-ion distribution was calculated in TRANSP, and an example of the distribution versus pitch-angle and energy

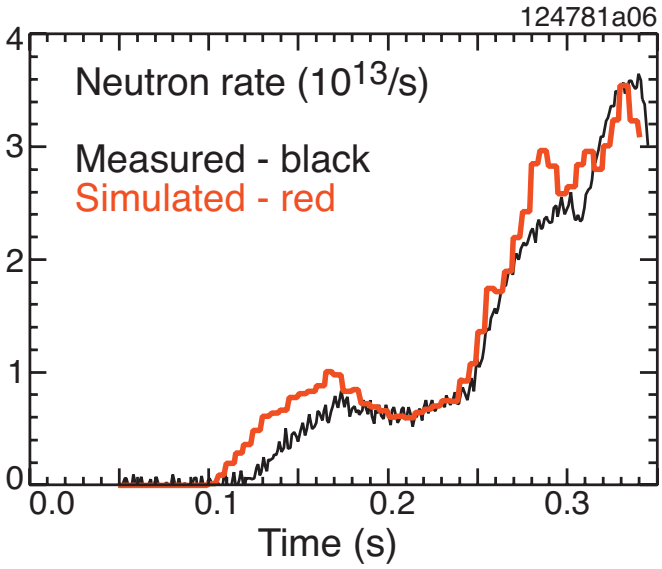

FIG. 9. (Color) TRANSP simulation of neutron rate (in red) assuming He prefill, injection of deuterium neutral beams and recycling of 13% D, and 87% He compared to measured rate (black).

is shown in Fig. 10. This distribution is taken at the radius near the minimum in q and has a peak at full energy with a pitch, $V_{\|}/V \approx 0.75$. The width of the peak broadens as the ions slow down due to pitch-angle scattering. Nearer the magnetic axis the peak at full energy in pitch is ≈0.5. The dashed line in the figure shows where $V_{\|} \approx V_{\text{Alfvén}}$ (note that ions with energy as low as 10 keV can meet this resonance condition). These fast-ion distributions of course do not incorporate how the TAE or TAE avalanches affect fast-ion transport.

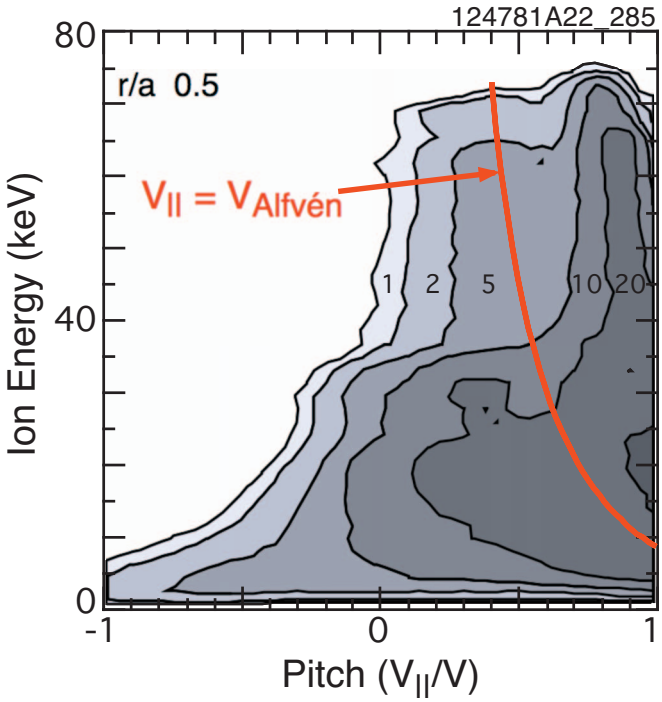

FIG. 10. (Color) Ion distribution function at r/a≈0.5 on the outboard midplane as calculated in TRANSP.

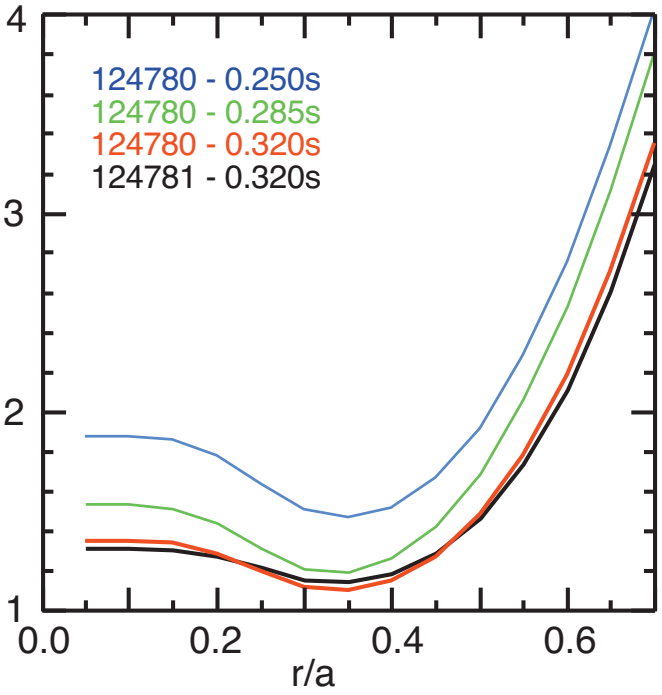

FIG. 11. (Color) q-profiles from LRDFIT equilibrium reconstructions at time of initial TAE activity, 0.25 s (blue), at time of avalanche being analyzed, 0.285 s (green), and comparison of q-profiles for shots 124 780 (red) and 124 781 (black).

The evolution of the q-profile was measured from 0.1 to 0.17 s, and again after about 0.3 s in the plasma shot being discussed here. TRANSP may be used to calculate the current relaxation in the period from 0.17 to 0.3 s, but the q-profile evolution from a similar shot with MSE data during the time of interest was used for the following analysis. A comparison of the q-profiles at 0.32 s from the two shots is shown in Fig. 11 (red and black curves) and the q-profiles at roughly the beginning of TAE activity (blue) and at the time of the avalanche being studied in detail here (green).

IV. NOVA ANALYSIS

The ideal NOVA stability code finds stable and unstable ideal eigenmodes, Fourier decomposed in the poloidal and toroidal directions. The NOVA-K code calculates the perturbative fast-ion drive and the Landau, radiative and resistive damping rates. The goal of the present analysis of the TAE bursts is to use these experiments to benchmark the ORBIT code simulations of fast-ion losses, so comparisons of NOVA-K stability predictions (as in, for example, Ref. 48) to experimental onset thresholds will be deferred to a future publication. The first step in modeling the fast-ion transport was to find the eigenmode structure with the NOVA ideal stability code. For input to NOVA, the plasma equilibrium was reconstructed during the avalanching period using the equilibrium code, LRDFIT, and the kinetic pressure profile was calculated with the TRANSP code, which includes thermal ion and electron, as well as the fast-ion pressure profiles.

The NOVA code has at least four significant limitations for modeling the TAE structure needed as input to ORBIT. The first is that the eigenmodes modeled with NOVA use a finite number of poloidal harmonics (here, Np=50) thus the eigenfunction can only be accurately modeled for $q(a) < Np/n$, where n is the toroidal mode number. This is of concern for high toroidal mode numbers generally, and particularly for modes in diverted plasmas where q becomes large near the edge. Second, important for NSTX and spherical tokamaks in general, NOVA does not fully include the physics of sheared plasma rotation. For NSTX, core rotation frequencies very typically approach 30 kHz on axis, whereas the TAE frequencies are in the range of from 60 kHz to 80 kHz. Thus, the rotation would have significant impact on the radial shape of the gap. Third, NOVA lacks the spatial resolution and appropriate physics to accurately model the TAE interaction with the continuum. Even at the low aspect ratio of NSTX, with concomitant wide TAE gap, many eigenmodes interact with the continuum near the axis, and in some cases near the plasma edge. Including the sheared rotation, to first order, distorts the TAE gaps so that they are fully closed in typical NSTX plasmas. Finally, the eigenmodes calculated with NOVA are from a linear, perturbative code; perturbative in the sense that the interaction with the fast-ion population is treated perturbatively and does not affect the structure of the eigenmodes. In the experiment, reflectometer measurements suggest that the mode structure is relatively unchanged during growth and saturation, however, strong downward frequency chirping is commonly observed, suggesting that the fast-ion distribution is affecting the frequency, if not the structure, of the eigenmodes. In the following analysis, we first start by neglecting rotation and explore the sensitivity of the eigenmodes to their changing interaction with the continuum for the same equilibrium on different coordinate systems.

A. NOVA eigenmode dependence on coordinate system

NOVA has three choices for the numerical grid, the "equal arcs" poloidal representation, "Boozer" coordinates, and "PEST" coordinates. The first, "equal arcs," is preferred for NOVA calculations as it has intrinsically better spatial resolution in the core. However, the "Boozer" coordinate system is less susceptible to numerical problems for particle following codes and is desired for ORBIT. Thus, we explored NOVA analysis in both the equal arc and Boozer coordinate systems. The default 151 point radial grid can be doubled to 301 points for higher radial resolution calculations. It is found that changing the coordinate system results in a different set of eigenmodes, most likely because the numerical interaction of the modes with the Alfvén continuum is changed. From Fig. 12 it should also be noted that, while NSTX is "low" aspect ratio and the TAE "gap" should be correspondingly wide, the region near the axis remains, of course, "high" aspect ratio and the gap can be quite small in this region, depending sensitively on how close q(0) is to rational. Thus, even in this low-aspect ratio geometry, many of these eigenmode solutions intersect the continuum.

We begin discussion of the analysis with the reference equilibrium, taken at 0.285 s or the time of the fourth TAE burst. The sheared rotation is neglected, and the NOVA analy-

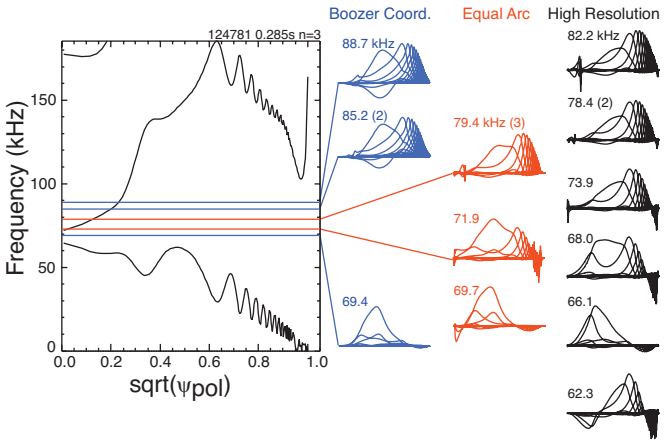

FIG. 12. (Color) Continuum as calculated with NOVA for the n=3 modes. Also shown, on right, are representative eigenmode solutions. Solutions found in Boozer coordinates (blue), equal arc coordinates (red), and higher resolution equal arc coordinates (black).

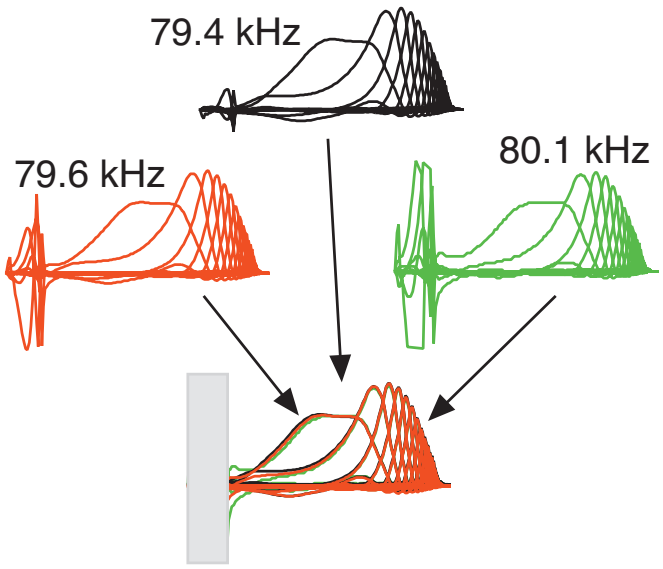

FIG. 13. (Color) Three "degenerate" eigenmodes of the equal arcs solutions shown in Fig. 11.

sis at this time will be focused on the dominant, n=3, TAE, comparing results from calculations done in Boozer coordinates, equal arc coordinates, and double-resolution equal arc coordinates. The equal arc coordinate gap structure (essentially the same in all coordinate systems) is shown in Fig. 12. On the right-hand-side of the figure are shown graphical representations of the ideal poloidal-harmonic contributions to the flux surface displacement found in the different coordinate systems for this equilibrium. The first column (blue) shows the eigenmodes found in the Boozer coordinates, while the second column (red) shows equal arc eigenmodes and the last (black) those for equal arc with double radial resolution. While, in principle, the solutions should be independent of the choice of coordinate system (apart from different distributions of poloidal harmonics), spatial resolution limitations where the modes interact with the continuum can subtly affect the eigenfrequency and eigenmode structure. Modes whose amplitude is small at their intersection with the continuum may be assumed to be minimally affected, and thus represent a reasonably accurate approximation to true eigenmodes. Eigenmodes that showed very strong interactions with the continuum are omitted here.

For the three coordinate systems, modes with frequencies from 68 to 90 kHz are found with qualitatively similar "TAE-like" radial structures. However, different sets of eigenmodes are found for each of the coordinate systems. All of these eigenmode solutions intersect the continuum near the axis. Qualitatively similar reverse-shear Alfvén eigenmode (rsAE)-like modes,[109–118] whose frequency sits in the gap from the core to the edge, are found at 69.4 kHz in Boozer coordinates, 69.7 kHz in equal arcs, and 66.1 kHz in high resolution equal arcs coordinates. Note that the structure of these modes, decomposed into different basis sets for the Boozer and equal arcs coordinate systems, is not expected to be the same. The "equal arc" and "high resolution" eigenvectors, however, should be the same. A reasonable interpretation is that the interaction with the continuum introduces numerical jumps in the radial mode structure, changing the eigenmode solutions.

The frequencies for the eigenmodes shown in Fig. 12 are indicated for each eigenmode in the upper left. The number in parentheses after some frequencies indicates the number of "degenerate" eigenmodes found at that frequency (modes with nearly the same frequency and structure), for which only one solution is shown. An example of mode degeneracy, which illustrates the numerical issues arising from the continuum interaction, is shown in Fig. 13. The mode at 79.4 kHz (Fig. 12, second column) is accompanied by similar solutions at 79.6 and 80.1 kHz, as shown in an arc across the top Fig. 13. The linear eigenmodes are scaled to match amplitudes in the outer part of the plasma and overlaid at the bottom of the figure. For the modes at 79.6 and 80.1 kHz, the mode amplitude inside the radius of continuum interaction is clipped to help illustrate that the outer eigenmode structures are nearly identical for these three modes; there are only small differences as the continuum is approached. The mode at 79.4 kHz is considered the most physical of the solutions as the mode amplitude is small at the continuum, thus in some sense the mode is less sensitive to the numerical problems at the continuum interaction point (for example, if a mode could be found with zero amplitude in the continuum region, there would be no interaction).

B. NOVA eigenmode dependence on equilibrium evolution

The eigenmode interactions with the continuum not only introduce numerical uncertainties in the calculation of the eigenmode structure, they also introduce a real and important damping term for the TAE. The equilibrium q-profile at the time of the fourth TAE burst analyzed in Fig. 12 happened to have $q(0) \approx 1.53$ on axis; close to the $q(0)=1.5$ which would have closed the gap on axis. Thus, as the q-profile evolves through the shot, it would be expected that the gap on axis opens and closes, affecting the threshold for exciting the TAE.

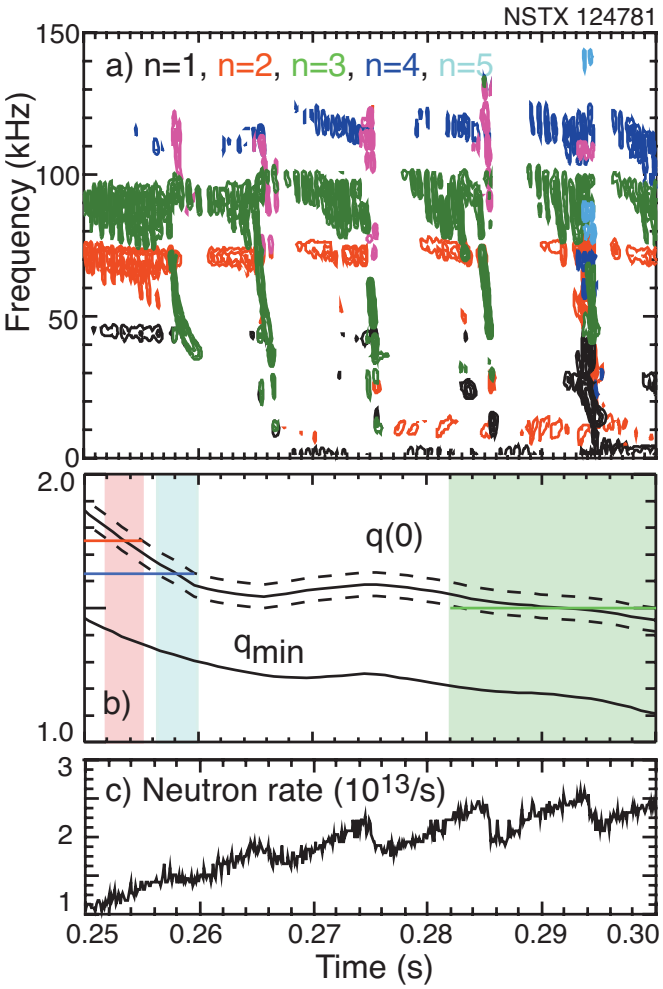

FIG. 14. (Color) (a) Spectrogram showing TAE activity. (b) Evolution of q(0) and q_{min} deduced from equilibrium reconstruction and (c) neutron rate.

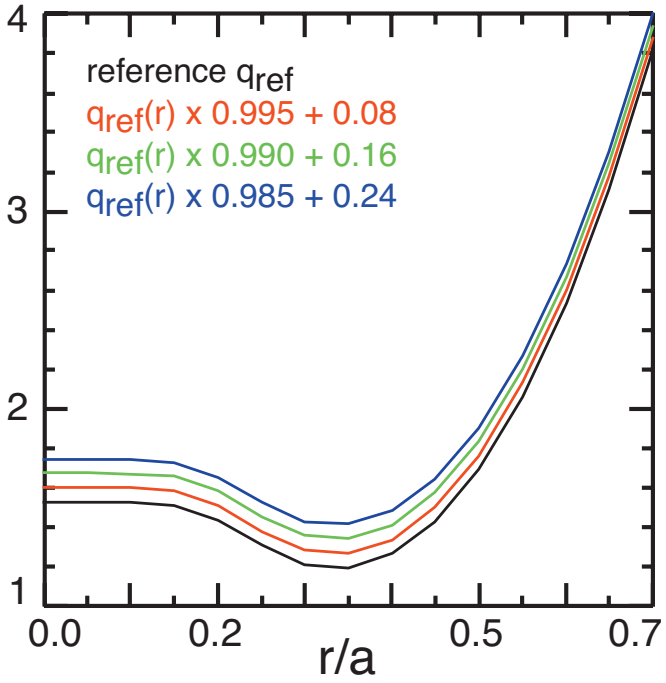

FIG. 15. (Color) Variations in the core q-profile for the NOVA simulations shown in Fig. 13.

The TAE onsets shortly after the current ramp ends, so the internal plasma current profile is still evolving. From the onset time of the TAE until the last of the strong bursts, the q-profile evolves, with $q(0) \approx 2$ at the start of TAE activity and $q(0) \approx 1.5$ by the last strong TAE burst (Fig. 14). The shaded regions of Fig. 14(b) indicate where the n=2 (red), n=3 (green), and n=4 (blue) gaps should be nearly closed on axis. While there is perhaps some correlation for the amplitude of the n=4 modes, the q-profile evolution appears to have little effect on the n=2 and n=3 modes.

NOVA simulations were done for equilibria roughly spanning the range in q-profiles from the first strong TAE burst at 0.257 s to the fourth burst at 0.285 s, not quite the full range in q-profiles between the blue and green curves in Fig. 11. For these simulations, all that was varied was the q-profile in the center of the plasma (Fig. 15). As indicated in the figure, the reference q-profile was scaled by a constant factor, then offset to keep $q(a) \approx$ constant, for example, $q_b(r) = 0.990\, q_{ref}(r) + 0.16$ (the green curve).

The n=3 continua, as calculated in NOVA, are shown in Fig. 16. Notice that the gap is nearly closed on axis for the reference q-profile (black), but opens substantially for the "earlier" q-profiles (red, green and blue). As before, not all eigenmodes could be "tracked" through the equilibrium changes. The modes clearly in the gap fared best, with the mode at 69.4 kHz in the reference case (black) apparently persisting throughout the q-evolution. The TAE-like solutions above 80 kHz, which intersected the continuum near the core could only be found for the reference and the "second avalanche" q-profiles.

C. NOVA eigenmodes with Doppler shift corrections to continuum

Central rotation frequencies in NSTX are typically a substantial fraction of the TAE central gap frequency, so including Doppler-frequency corrections to the TAE gap structure result in substantial radial distortion of the Alfvén continuum. The measured core rotation frequency of ≈30 kHz closes the n=3 TAE gap. A version of NOVA was created

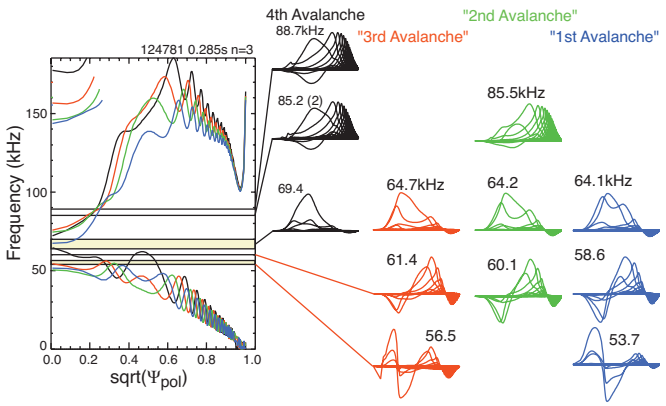

FIG. 16. (Color) Continuum corresponding to the four q-profile variations shown in Fig. 12. The corresponding eigenmodes for each q-profile are shown to the right (labeled by the frequency in kilohertz).

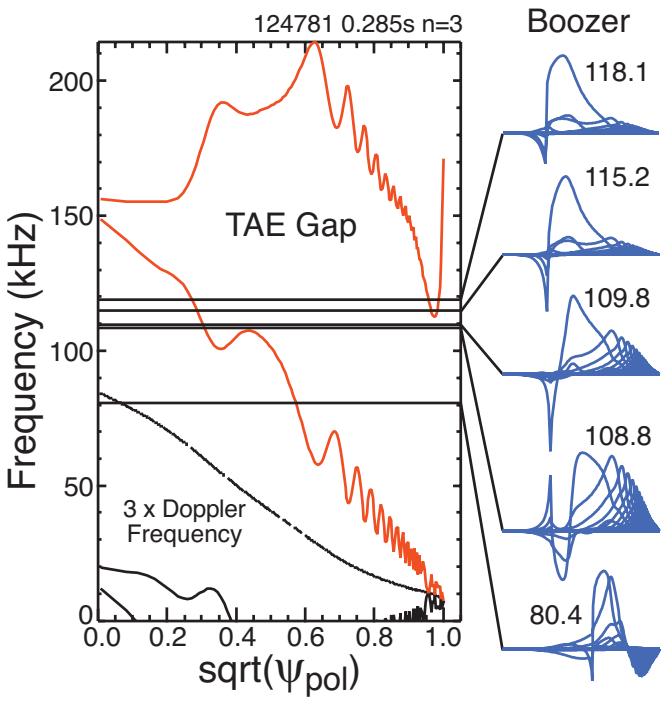

FIG. 17. (Color) TAE gap corrected for sheared rotation. Eigenmodes are shown to the right; the numbers indicate the frequency in kilohertz.

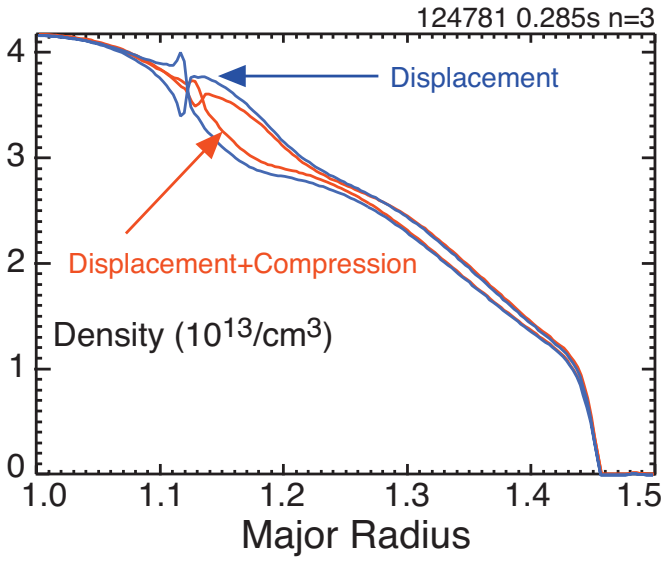

FIG. 18. (Color) Simulated density profiles at peak and minimum for mode at half of the peak amplitude: blue—density perturbation from displacement, red—density perturbation from displacement and compression, scaled up by 2.

which includes some of the physical effects of sheared rotation.[119] The continuum for the n=3 gap including the sheared rotation is shown in Fig. 17.

The five eigenmode solutions that were found for this gap structure are shown on the right. Each of them has strong interactions with the continuum. The stronger interaction with the continuum results in greater variation of radial structure than for the cases without the Doppler correction. The strength of the interaction with the continuum in NOVA is sensitive to the location of the continuum crossing relative to the analysis grid; even very small equilibrium changes modify the size of the (unphysical) jumps in the eigenfunction, changing the eigenfrequency. This makes interpretation of a study of the sensitivity to q-profile evolution difficult with NOVA.

The two highest frequency modes shown, 115.2 and 118.1 kHz, have eigenfunctions with some similarities to rsAE. As with rsAE, the poloidal harmonic (m=4) of the TAE localized to the wide, low shear region, reaches a relatively large amplitude. However, the m=5 poloidal harmonic remains strongly coupled and the mode amplitude is not as localized to the q_{min} region as for the rsAE studied in lower β NSTX plasmas [cf. Crocker *et al.*, Ref. 118, Figs. 10 and 11]. The estimated GAM frequency at q_{min}, $\approx$100 kHz, is comparable to even the Doppler-shifted TAE frequency, so rsAE would be expected to be suppressed.[117] The evolution of the amplitude, frequency and mode structure of the n=3 TAE shows no sensitivity to the evolution of q_{min} (e.g., Fig. 14), as would be expected for rsAE. Thus, while these modes might be considered to be a hybrid mixture of coupled TAE and rsAE, the TAE characteristics are dominant.

D. Comparison of NOVA eigenmodes with reflectometer data

The simplest description of the functioning of a reflectometer is that the wave reflects off of the cutoff layer and a measurement of the phase shift of the reflected signal is interpreted to give the change in distance to the cutoff layer. Thus the reflectometer measures directly the internal displacement of the plasma constant density (flux surface) due to the mode. The mode profile data from the reflectometer will be presented using this simple conversion (the "long wavelength" approximation) of the phase-shift data to displacement (the measured phase shifts are converted to displacements using double the free-space wavelength). However, there is also a phase shift due to the change in the line integral plasma density between the cutoff layer and the plasma edge. A more accurate interpretation of the reflectometer signal uses a numerical simulation using the NOVA radial structure of the mode and the measured plasma density profile.

The NOVA code calculates ideal poloidal harmonic contributions to the flux surface displacement for the eigenmodes. The displacement is used to calculate the perturbed density profile on the outboard midplane (Fig. 18). The phase shifts resulting from the density perturbations are then calculated for a range of reflectometer frequencies. The perturbed density in Fig. 18 is shown for calculations using just the mode displacement (blue), and also for the mode displacement together with compressional corrections (red). The profile shape is not significantly changed by the inclusion of the compressional terms, but the mode amplitude needed to match the reflectometer data is increased by a factor of roughly 2 (on the outboard midplane where the reflectometer measurements are made) with the compressional corrections. Comparison to the reflectometer data using displacement

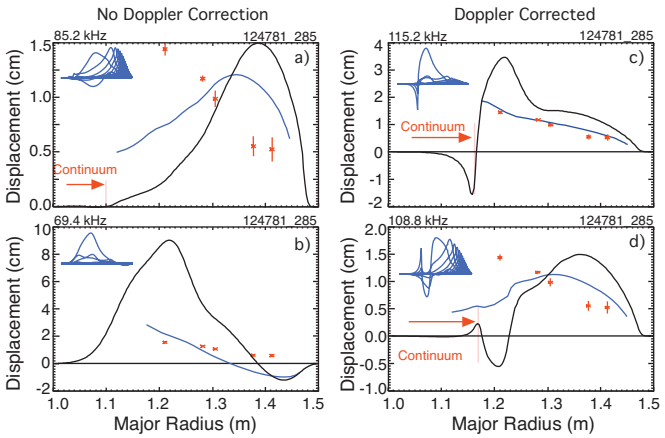

FIG. 19. (Color) Comparison of reflectometer data with NOVA eigenmode structures for four n=3 modes: (a) 85.2 kHz with no Doppler corrections, (b) 69.4 kHz with no Doppler corrections, (c) 115.2 kHz with Doppler corrections, and (d) 108.8 kHz with Doppler correction.

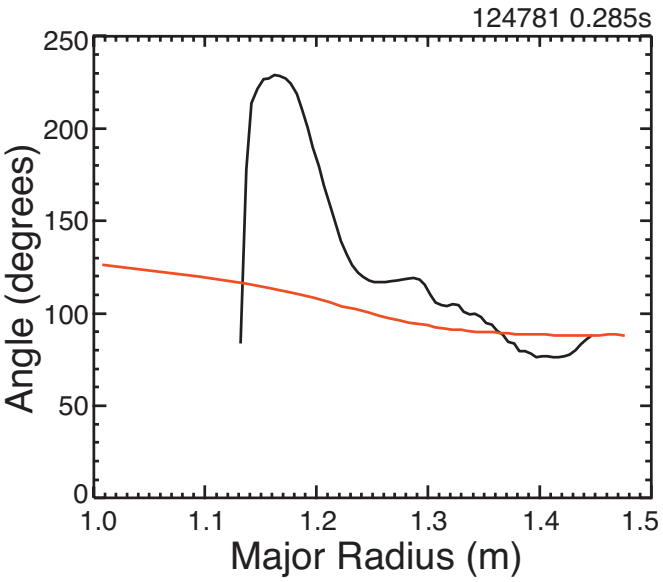

FIG. 20. (Color) Pitch of n=3 magnetic fluctuations relative to equilibrium field; black–NOVA and red-experiment.

only is easier and is used to choose and scale the NOVA eigenmodes for the ORBIT code.

Four examples of n=3 eigenmodes from NOVA simulations are compared with the reflectometer data in Fig. 19. The solid blue curve is the simulated reflectometer response ("synthetic reflectometer diagnostic") and the five experimental points from the reflectometer array are shown in red. The experimental data represent an average of ten measurements of the radial mode structure during the final burst. In Figs. 19(a) and 19(b) two of the eigenmodes calculated without Doppler frequency corrections are compared with the profiles for the n=3 mode. The five reflectometer data points are sufficient to reject these eigenmodes as poor fits. Of the two representative eigenfunctions calculated with the Doppler correction to the radial Alfvén continuum, the higher frequency calculation is found to be a good fit. The fit also provides the factor by which to scale the NOVA eigenmode to match the experimental mode amplitude.

The angle of the perturbed magnetic field relative to the equilibrium field in the flux surface is calculated on the outboard midplane for the n=3 NOVA eigenmode. The local angle is shown as the black curve in Fig. 20. Where the angle is 90°, the mode has pure "shear" polarity, as opposed to compressional polarity. For comparison, the relative angle between the measured magnetic fluctuation at the wall and the equilibrium field is shown in red. The measured pitch would be expected to be dominated by the pitch of the edge harmonics for TAE, which is nearly perpendicular to the edge equilibrium field. But for modes where the perturbed currents are more internally localized, such as tearing modes, the edge magnetic fluctuation pitch reflects the pitch of the perturbed currents, or equilibrium field, at the rational surface.

The NOVA code was used to find eigenmode solutions for the other two important TAE modes seen in the avalanche at 0.285 s. The dominant mode is the n=3 mode, described above. There is an n=6 mode, but it appears to be a harmonic of the n=3, so its role in the fast-ion transport is not clear. NOVA found multiple solutions for both the n=2 and n=4 modes for the Doppler-corrected equilibrium. The best fits to the reflectometer array data are shown in Fig. 21. The signal-to-noise level for the outer points of the n=2 modes is not that good, and the disagreement with the outermost point is not of concern. Phase information is indicated by positive and negative displacements, as the NOVA eigenmodes and the experimental data typically showed either no radial phase shifts (as in Fig. 19) or 180° phase jumps for some of the other modes. The n=4 mode has a phase inversion, which is reproduced for the NOVA eigenmode. These eigenmodes are also found for the continuum calculated including sheared-Doppler corrections.

V. ORBIT ANALYSIS OF THE FAST-ION TRANSPORT

The ORBIT code is used to model the effect of the TAE on fast-ion transport. The ORBIT code calculates the guiding-center orbits of fast ions in the experimental equilibrium in the presence of multiple TAE. The TAE avalanche was simulated by using the linear eigenmode structure as simulated with NOVA for the n=2, n=3, and n=4 modes. For each of the modes, the measured amplitude and frequency evolution over the 1 ms of the final, large avalanche burst were used in the simulation. The amplitude evolution of the n=3 mode was approximated with a linear ramp in time, and the frequency evolution was modeled with a linear downward frequency chirp from 85 to 33 kHz (approximating the Doppler correction). The n=2 and n=4 modes were modeled with constant amplitude and frequency. ORBIT simulations were run with 1000 ions representing the fast-ion distribution calculated with the TRANSP Monte Carlo beam deposition package.

The ORBIT simulation of the TAE burst found that roughly 12% of the fast ions were lost during the 1 ms burst (Fig. 22). The fast ions are considered lost when their guiding center moves outside the last closed flux surface. No

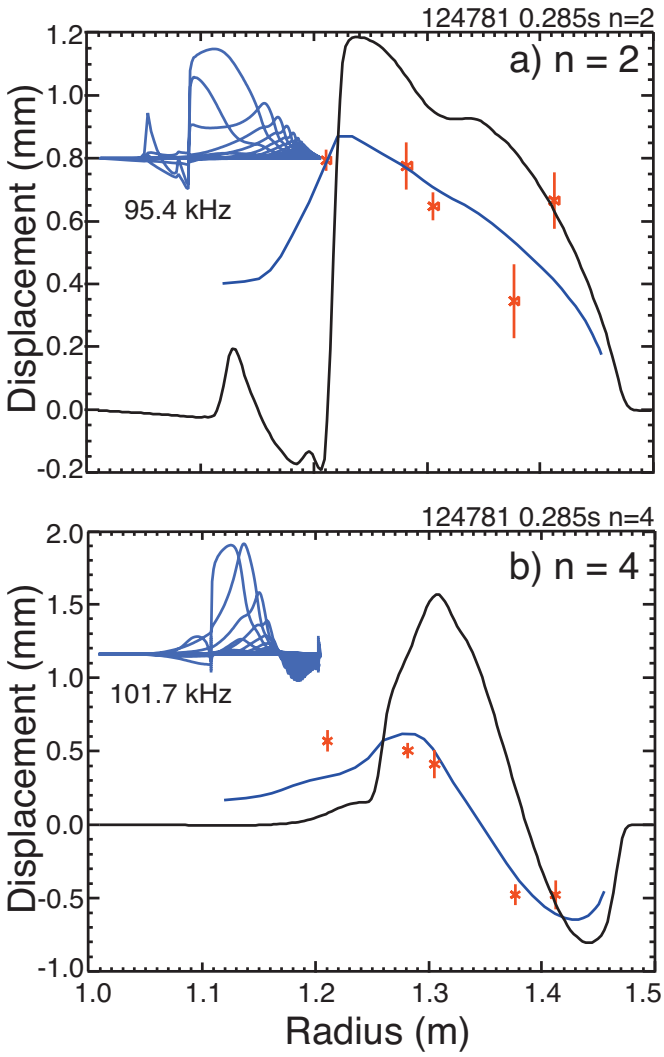

FIG. 21. (Color) Best NOVA eigenmode fits for the n=2 and n=4 modes.

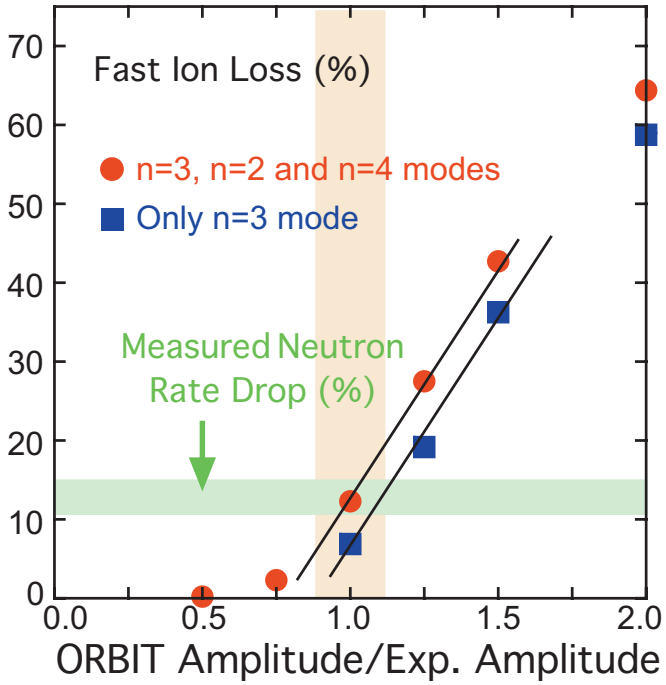

FIG. 22. (Color) The percent of fast ions lost vs normalized mode amplitudes (red), losses with only n=3 mode (blue).

attempt is made to follow the orbits outside the last closed surface, or to model actual vacuum vessel structures. Additional simulations were run with mode amplitudes ranging from half to up to six times the experimentally measured amplitudes. At one-half of the observed mode amplitudes, the fast-ion losses are negligible, but show a strong, nonlinear onset at an amplitude of ≈80% of the experimental amplitude. Above the threshold, the loss scales in an offset linear fashion with mode amplitude as loss(%)≈61*(A_N−0.8), where A_N is the mode amplitude used in ORBIT, normalized to the measured amplitude. The loss rate begins to saturate above about 50% loss, or above an amplitude of ≈1.6 times the measured amplitude. A simulation done with only the dominant, n=3 mode showed a similar behavior, albeit with the threshold for onset of losses increased to a normalized amplitude of ≈0.9.

The observed drop in the neutron rate is ≈12%, which would correspond to a loss of ≈12% of fast ions (across all energies) if the neutron production was from beam-target reactions, or ≈6% if neutron production was primarily from beam-beam reactions. The neutron production in these NSTX helium plasmas is approximately 60% beam-beam and 40% beam target. The fast-ion loss can be estimated as $\delta S/S \approx 0.6\times 2\times \delta n_{fast}/n_{fast} + 0.4\times \delta n_{fast}/n_{fast} \approx 1.6\,\delta n_{fast}/n_{fast}$, or about 7.5%.

Simulations were also done with fast-ion populations with energies limited to ranges from 10 to 25 keV, 25 to 40 keV, 40 to 55 keV, and 55 to 70 keV to determine the energy dependence of the fast-ion losses. A larger fraction is lost at lower energies, ranging from somewhat more than 12% of the lower energy fast ions to ≈6.5% of the most energetic fast ions (Fig. 23). This implies that the drop in neutron rate would be less than a direct proportionality to the fast-ion losses. However, the strong dependence of fast-ion losses on mode amplitude means that the simulations are still in qualitative agreement.

A dependence of losses on the frequency of the n=3 mode is also seen. For simulations where the frequency chirp from 85 to 33 kHz was replaced by a constant frequency of 85 kHz, the losses were substantially higher. At 33 kHz the losses were less than with the frequency chirp. The ORBIT simulations were done without including the rotational shear, and this result suggests that inclusion of this effect may significantly change the resonant interactions of fast ions with the mode.

The strong offset linear increase in losses is consistent with an island overlap threshold or avalanche model as proposed by Berk, *et al.*[97] The experimental measurements of the mode amplitudes are at the threshold for strong, nonlinear losses. A 20% increase in amplitude could more than double the losses and a reduction in amplitude by 20% would reduce losses to a negligible level. That there is a similar strong threshold, at larger amplitude, for the simulations with a single mode is not surprising in that TAE can

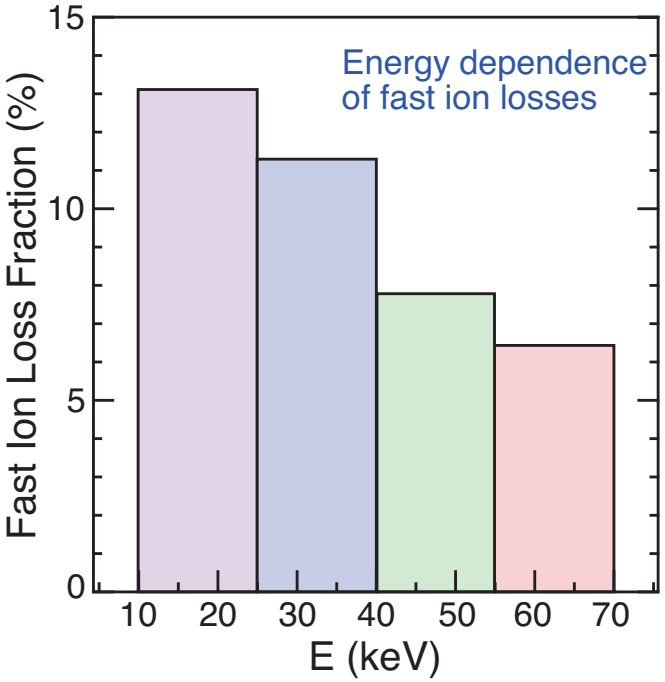

FIG. 23. (Color) The four bars indicate percentages of fast-ion losses in the indicated energy ranges.

have multiple phase space resonances with fast ions. Thus, even for a single mode, overlap of multiple phase-space islands is possible at large amplitude.

VI. SUMMARY

In this work we demonstrated that the NOVA code can provide reasonable, qualitative models of the TAE structure consistent with the measurements by the five channel reflectometer array. While the NOVA code found eigenmodes with frequencies and radial structure matching the experimental measurements, it also found many additional modes not seen in the experiments. The eigenmodes found were sensitive to the coordinate system used and to small changes in the equilibrium. This sensitivity is believed to result from insufficient numerical resolution and an incomplete physics model where the mode interacts with the continuum. Finally, the sheared rotation in NSTX introduces a frequency shear between the core and edge of ≈25 kHz, a significant fraction of the gap center frequency. The distortion of the continuum, or gap structure, by this sheared rotation means that despite the low aspect ratio of NSTX, the TAE gaps are typically "closed." Indeed, the best fits to the measurements of the radial mode structure were found with a model including some of the physics of sheared rotation.

ORBIT simulations with the linear NOVA eigenmodes scaled to match the experimental mode amplitudes and frequencies predict a loss of ≈12% of the fast-ion population through a simulated 1 ms avalanche burst. The measured drop in the neutron rate was also ≈12%, but comparison of these numbers is complicated by the energy dependence of the fast-ion losses in the ORBIT simulations and by the mix of beam-beam and beam-target neutrons in the experiment. Further simulations indicate that the losses are not linear with mode amplitude, but approximately offset linear with a threshold amplitude just below the experimental amplitude.

These simulations are not self-consistent and there are important physical effects missing from the codes. Inclusion of the physics of sheared rotation is important for analysis and predictions in the ST geometry where the low field and high density reduce the Aflvén speed to of order the toroidal rotation velocity. The TAE in NSTX appear to interact strongly with the continuum and an improved model of this interaction is needed for realistic modeling of the TAE. The strong frequency chirping seen in NSTX is an inherently nonlinear effect probably best modeled in a nonlinear code such as M3D-K, although the experimental evidence suggests that the mode structure is not strongly modified by the frequency chirp. Finally, the guiding-center approximation in ORBIT may not be adequate for NSTX with its intrinsically large ρ^* and future work will explore full-orbit calculations.

ACKNOWLEDGMENTS

This work was supported by U.S. DOE Contract Nos. DE-AC02-09CH11466, DE-FG03-99ER54527, DE-FG02-06ER54867, and DE-FG02-99ER54527.

[1] E. D. Fredrickson, R. Bell, D. Darrow, G. Fu, N. Gorelenkov, B. LeBlanc, S. Medley, J. Menard, H. Park, L. Roquemore, S. A. Sabbagh, D. Stutman, K. Tritz, N. Crocker, S. Kubota, W. Peebles, K. C. Lee, and F. Levinton, Phys. Plasmas **13**, 056109 (2006).
[2] M. Ono, S. M. Kaye, Y.-K. M. Peng, G. Barnes, W. Blanchard, M. D. Carter, J. Chrzanowski, L. Dudek, R. Ewig, D. Gates, R. E. Hatcher, T. Jarboe, S. C. Jardin, D. Johnson, R. Kaita, M. Kalish, C. E. Kessel, H. W. Kugel, R. Maingi, R. Majeski, J. Manickam, B. McCormack, J. Menard, D. Mueller, B. A. Nelson, B. E. Nelson, C. Neumeyer, G. Oliaro, F. Paoletti, R. Parsells, E. Perry, N. Pomphrey, S. Ramakrishnan, R. Raman, G. Rewoldt, J. Robinson, A. L. Roquemore, P. Ryan, S. Sabbagh, D. Swain, E. J. Synakowski, M. Viola, M. Williams, J. R. Wilson, and NSTX Team, Nucl. Fusion **40** 557 (2000).
[3] W. W. Heidbrink, K. Bol, D. Buchenauer, R. Fonck, G. Gammel, K. Ida, R. Kaita, S. Kaye, H. Kugel, B. LeBlanc, W. Morris, M. Okabayashi, E. Powell, S. Sesnic, and H. Takahashi, Nucl. Fusion **23**, 917 (1983).
[4] L. Chen, R. B. White, and M. N. Rosenbluth, Phys. Rev. Lett. **52**, 1122 (1984).
[5] G. Y. Fu and C. Z. Cheng, Phys. Fluids B **4**, 3722 (1992).
[6] S. J. Zweben, C. E. Bush, C. S. Chang, Z. Chang, D. S. Darrow, E. D. Fredrickson, H. W. Herrmann, H. E. Mynick, J. Schivell, M. Bell, R. Boivin, R. V. Budny, C. Z. Cheng, D. Ernst, G. Hammett, L. C. Johnson, D. McCune, M. Murakami, D. K. Owens, J. Park, C.-K. Phillips, M. H. Redi, S. Scott, J. D. Strachan, G. Taylor, M. Tuszewski, R. B. White, J. R. Wilson, and M. Zarnstorff, Phys. Plasmas **1**, 1469 (1994).
[7] H. H. Duong, W. W. Heidbrink, E. J. Strait, T. W. Petrie, R. Lee, R. A. Moyer, and J. G. Watkins, Nucl. Fusion **33**, 749 (1993).
[8] H. H. Duong and W. W. Heidbrink, Nucl. Fusion **33**, 211 (1993).
[9] H. Kimura, M. Saigusa, S. Moriyama, T. Kondoh, Y. Neyatani, T. Ozeki, T. Nishitani, Y. Kusama, T. Fujii, M. Sato, M. Nemoto, K. Tobita, and C. Z. Cheng, Phys. Lett. A **199**, 86 (1995).
[10] R. B. White, E. Fredrickson, D. Darrow, M. Zarnstorff, R. Wilson, S. Zweben, K. Hill, Y. Chen, and G. Fu, Phys. Plasmas **2**, 2871 (1995).
[11] D. S. Darrow, S. J. Zweben, Z. Chang, C. Z. Cheng, M. D. Diesso, E. D. Fredrickson, E. Mazzucato, R. Nazikian, C. K. Phillips, S. Popovichev, M. H. Redi, R. B. White, J. R. Wilson, and K. L. Wong, Nucl. Fusion **37**, 939 (1997).
[12] S. J. Zweben, D. S. Darrow, E. D. Fredrickson, G. Taylor, S. von Goeler, and R. B. White, Nucl. Fusion **39**, 1097 (1999).
[13] S. J. Zweben, R. V. Budny, D. S. Darrow, S. S. Medley, R. Nazikian, B. C. Stratton, E. J. Synakowski, and G. Taylor, Nucl. Fusion **40**, 91 (2000).
[14] E. M. Carolipio, W. W. Heidbrink, C. Z. Cheng, M. S. Chu, and G. Y. Fu, Phys. Plasmas **8**, 3391 (2001).

[15]E. D. Fredrickson, C. Z. Cheng, D. Darrow, G. Fu, N. N. Gorelenkov, G. Kramer, S. S. Medley, J. Menard, L. Roquemore, and D. Stutman, and R. B. White, Phys. Plasmas **10**, 2852 (2003).
[16]S. S. Medley, N. N. Gorelenkov, R. Andre, R. E. Bell, D. S. Darrow, E. D. Fredrickson, S. M. Kaye, B. P. LeBlanc, and A. L. Roquemore, Nucl. Fusion **44**, 1158 (2004).
[17]M. R. Tournianski, R. J. Akers, P. G. Carolan, and D. L. Keeling, Plasma Phys. Controlled Fusion **47**, 671 (2005).
[18]W. W. Heidbrink, M. A. Van Zeeland, M. E. Austin, K. H. Burrell, N. N. Gorelenkov, G. J. Kramer, Y. Luo, M. A. Makowski, G. R. McKee, C. Muscatello, R. Nazikian, E. Ruskov, W. M. Solomon, R. B. White, and Y. Zhu, Nucl. Fusion **48**, 084001 (2008).
[19]K. McGuire, R. Goldston, M. Bell, M. Bitter, K. Bol, K. Brau, D. Buchenauer, T. Crowley, S. Davis, F. Dylla, H. Eubank, H. Fishman, R. Fonck, B. Grek, R. Grimm, R. Hawryluk, H. Hsuan, R. Hulse, R. Izzo, R. Kaita, S. Kaye, H. Kugel, D. Johnson, J. Manickam, D. Manos, D. Mansfield, E. Mazzucato, R. McCann, D. McCune, D. Monticello, R. Motley, D. Mueller, K. Oasa, M. Okabayashi, K. Owens, W. Park, M. Reusch, N. Sauthoff, G. Schmidt, S. Sesnic, J. Strachan, C. Surko, R. Slusher, H. Takahashi, F. Tenney, P. Thomas, H. Towner, J. Valley, and R. White, Phys. Rev. Lett. **50**, 891 (1983).
[20]R. B. White, R. J. Goldston, K. McGuire, A. H. Boozer, D. A. Monticello, and W. Park, Phys. Fluids **26**, 2958 (1983).
[21]J. D. Strachan, B. Grek, W. Heidbrink, D. Johnson, S. M. Kaye, H. W. Kugel, B. LeBlanc, and K. McGuire, Nucl. Fusion **25**, 863 (1985).
[22]W. W. Heidbrink, K. Bol, D. Buchenauer, R. Fonck, G. Gammel, K. Ida, R. Kaita, S. Kaye, H. Kugel, B. LeBlanc, W. Morris, M. Okabayashi, E. Powell, S. Sesnic, and H. Takahashi, Phys. Rev. Lett. **57**, 835 (1986).
[23]R. Betti and J. P. Freidberg, Phys. Rev. Lett. **70**, 3428 (1993).
[24]Ya. I. Kolesnichenko, V. S. Marchenko, and R. B. White, Phys. Plasmas **8**, 3143 (2001).
[25]Y. Wu, C. Z. Cheng, and R. B. White, Phys. Plasmas **1**, 3369 (1994).
[26]E. D. Fredrickson, L. Chen, and R. B. White, Nucl. Fusion **43**, 1258 (2003).
[27]R. Kaita, R. B. White, A. W. Morris, E. D. Fredrickson, K. M. McGuire, S. S. Medley, T. J. Murphy, and S. D. Scott, Phys. Fluids B **2**, 1584 (1990).
[28]W. W. Heidbrink, Plasma Phys. Controlled Fusion **37**, 937 (1995).
[29]M. F. F. Nave, D. J. Campbell, E. Joffrin, F. B. Marcus, G. Sadler, P. Smeulders, and K. Thomsen, Nucl. Fusion **31**, 697 (1991).
[30]S. Günter, A. Gude, K. Lackner, M. Maraschek, S. Pinches, S. Sesnic, R. Wolf, and ASDEX Upgrade Team, Nucl. Fusion **39**, 1535 (1999).
[31]Ya. I. Kolesnichenko, V. S. Marchenko, and R. B. White, Phys. Plasmas **13**, 052504 (2006).
[32]W. W. Heidbrink, E. Ruskov, E. D. Fredrickson, N. Gorelenkov, S. S. Medley, H. L. Berk, and R. W. Harvey, Plasma Phys. Controlled Fusion **48**, 1347 (2006).
[33]D. S. Darrow, S. S. Medley, A. L. Roquemore, W. W. Heidbrink, A. Alekseyev, F. E. Cecil, J. Egedal, V. Ya. Goloborod'ko, N. N. Gorelenkov, M. Isobe, S. Kaye, M. Miah, F. Paoletti, M. H. Redi, S. N. Reznik, A. Rosenberg, R. White, D. Wyatt, and V. A. Yavorskij, in *Proceedings of the 19th IAEA Fusion Energy Conference*, Lyon, France, 14–19 October 2002 (IAEA, Vienna, 2003), CD-ROM file EX/P2-01 and available online at http://www-pub.iaea.org/MTCD/publications/PDF/csp_019c/START.HTM.
[34]H. L. Berk, C. J. Boswell, D. Borba, B. N. Breizman, A. C. A. Figueiredo, E. D. Fredrickson, N. N. Gorelenkov, R. W. Harvey, W. W. Heidbrink, T. Johnson, S. S. Medley, M. F. F. Nave, S. D. Pinches, E. Ruskov, S. E. Sharapov, and JET EFDA Contributors, in *Proceedings of the 21st IAEA Fusion Energy Conference*, Chengdu, China, 16–21 October 2006 (IAEA, Vienna, 2007), CD-ROM file TH/3-1 (available online at http://www.swip.ac.cn/xsyd/p1292/html/index.htm).
[35]J. P. Goedbloed, Phys. Fluids **18**, 1258 (1975).
[36]C. E. Kieras and J. A. Tataronis, J. Plasma Phys. **28**, 395 (1982).
[37]C. Z. Cheng and M. S. Chance, Phys. Fluids **29**, 3695 (1986).
[38]J. W. Van Dam, G. Fu, and C. Z. Cheng, Fusion Technol. **18**, 461 (1990).
[39]H. L. Berk, B. N. Breizman, and H. Ye, Phys. Lett. A **162**, 475 (1992).
[40]B. N. Breizman, H. L. Berk, and H. Ye, Phys. Fluids B **5**, 3217 (1993).
[41]H. L. Berk, J. W. Van Dam, D. Borba, J. Candy, G. T. A. Hysmans, and S. Sharapov, Phys. Plasmas **2**, 3401 (1995).
[42]H. L. Berk, B. N. Breizman, J. Fitzpatrick, and H. V. Wong, Nucl. Fusion **35**, 1661 (1995).
[43]H. L. Berk, B. N. Breizman, and M. Pekker, Nucl. Fusion **35**, 1713 (1995).
[44]H. L. Berk, B. N. Breizman, and M. Pekker, Phys. Rev. Lett. **76**, 1256 (1996).
[45]H. L. Berk, B. N. Breizman, J. Fitzpatrick, M. S. Pekker, H. V. Wong, and K. L. Wong, Phys. Plasmas **3**, 1827 (1996).
[46]H. L. Berk, B. N. Breizman, and M. Pekker, Plasma Phys. Rep. **23**, 778 (1997).
[47]N. N. Gorelenkov, Y. Chen, R. B. White, and H. L. Berk, Phys. Plasmas **6**, 629 (1999).
[48]N. N. Gorelenkov, C. Z. Cheng, G. Y. Fu, S. Kaye, R. White, and M. V. Gorelenkova, Phys. Plasmas **7**, 1433 (2000).
[49]N. N. Gorelenkov, E. V. Belova, H. L. Berk, C. Z. Cheng, E. Fredrickson, W. W. Heidbrink, S. Kaye, and G. J. Kramer, Phys. Plasmas **11**, 2586 (2004).
[50]G. Y. Fu, J. Breslau, E. Fredrickson, W. Park, and H. R. Strauss, in *Proceedings of the 20th International Conference on Plasma Physics and Controlled Nuclear Fusion Research*, Vilamoura, Portugal, 2004 (International Atomic Energy Agency, Vienna, 2005), CD-ROM file TH/P4-38.
[51]N. N. Gorelenkov, H. L. Berk, and R. V. Budny, Nucl. Fusion **45**, 226 (2005).
[52]R. B. White, Y. Wu, Y. Chen, E. D. Fredrickson, D. S. Darrow, M. C. Zarnstorff, J. R. Wilson, S. J. Zweben, K. W. Hill, G. Y. Fu, and M. N. Rosenbluth, Nucl. Fusion **35**, 1707 (1995).
[53]K. L. Wong, R. J. Fonck, S. F. Paul, D. R. Roberts, E. D. Fredrickson, R. Nazikian, H. K. Park, M. Bell, N. L. Bretz, R. Budny, S. Cohen, G. W. Hammett, F. C. Jobes, D. M. Meade, S. S. Medley, D. Mueller, Y. Nagayama, D. K. Owens, and E. J. Synakowski, Phys. Rev. Lett. **66**, 1874 (1991).
[54]K. L. Wong, R. Durst, R. J. Fonck, S. F. Paul, D. R. Roberts, E. D. Fredrickson, R. Nazikian, H. K. Park, M. Bell, N. L. Bretz, R. Budny, C. Z. Cheng, S. Cohen, G. W. Hammett, F. C. Jobes, L. Johnson, D. M. Meade, S. S. Medley, D. Mueller, Y. Nagayama, D. K. Owens, S. Sabbagh, and E. J. Synakowski, Phys. Fluids B **4**, 2122 (1992).
[55]R. D. Durst, R. J. Fonck, K. L. Wong, C. Z. Cheng, E. D. Fredrickson, and S. F. Paul, Phys. Fluids B **4**, 3707 (1992).
[56]J. R. Wilson, M. G. Bell, H. Biglari, M. Bitter, N. L. Bretz, R. Budny, C. E. Bush, L. Chen, Z. Chang, D. Darrow, P. C. Efthimion, E. Fredrickson, G. Y. Fu, R. Goldfinger, B. Grek, L. R. Grisham, G. Hammett, R. J. Hawryluk, D. Hoffman, J. C. Hosea, A. Janos, D. Jassby, F. C. Jobes, D. W. Johnson, L. C. Johnson, J. Machuzak, R. Majeski, D. K. Manasfield, E. Mazzucato, K. M. McGuire, S. S. Medley, D. Mueller, M. Murakami, R. Nazikian, D. K. Owens, H. Park, S. Paul, C. K. Phillips, A. T. Ramsey, D. Rasmussen, F. Rimini, J. H. Rogers, A. L. Roquemore, G. Schilling, J. Schivell, G. L. Schmidt, J. Stevens, B. C. Stratton, J. D. Strachan, E. Synakowski, G. Taylor, M. Ulrickson, K. L. Wong, M. Yamada, K. M. Young, M. C. Zarnstorff, and S. J. Zweben, in *Proceedings of the 14th International Conference on Plasma Physics and Controlled Nuclear Fusion Research*, Wurzburg, 1992 (IAEA, Vienna, 1993), Vol. I, p. 661, Paper No. IAEA-CN-56/E-2–2.
[57]G. Taylor, M. G. Bell, H. Biglari, M. Bitter, N. L. Bretz, R. Budny, L. Chen, D. Darrow, P. C. Efthimion, D. Ernst, E. Fredrickson, G. Y. Fu, B. Grek, L. Grisham, G. Hammett, J. C. Hosea, A. Janos, D. Jassby, F. C. Jobes, D. W. Johnson, L. C. Johnson, R. Majeski, D. K. Mansfield, E. Mazzucato, S. S. Medley, D. Mueller, Ft. Nazikian, D. K. Owens, S. Paul, H. Park, C. K. Phillips, J. H. Rogers, G. Schilling, J. Schivell, G. L. Schmidt, J. E. Stevens, B. C. Stratton, J. D. Strachan, E. Synakowski, J. R. Wilson, K. L. Wong, and S. J. Zweben, Phys. Fluids B **5**, 2437 (1993).
[58]K. L. Wong, J. R. Wilson, Z. Y. Chang, G. Y. Fu, E. Fredrickson, G. W. Hammett, C. Bush, C. K. Phillips, J. Snipes, and G. Taylor, Plasma Phys. Controlled Fusion **36**, 879 (1994).
[59]E. Fredrickson, Z. Y. Chang, R. V. Budny, C. Z. Chang, J. L. Dunlap, G. Y. Fu, A. Janos, E. Mazzucato, K. M. McGuire, R. Nazikian, K. L. Wong, and S. Zweben, in *Proceedings of the 15th International Conference on Plasma Physics and Controlled Fusion Research*, Seville, Spain, 1994 (International Atomic Energy Agency, Vienna, 2005), CD-ROM file CN-60/A-2-II-5.
[60]W. W. Heidbrink, J. Kim, and R. J. Groebner, Nucl. Fusion **28**, 1897 (1988).
[61]W. W. Heidbrink, E. J. Strait, E. Doyle, G. Sager, and R. T. Snider, Nucl. Fusion **31**, 1635 (1991).
[62]E. J. Strait, W. W. Heidbrink, A. D. Turnbull, M. S. Chu, and H. H. Duong, Nucl. Fusion **33**, 1849 (1993).
[63]W. W. Heidbrink, H. H. Duong, J. Manson, E. Wilfrid, and C. Oberman, Phys. Fluids B **5**, 2176 (1993).

[64]E. J. Strait, W. W. Heidbrink, and A. D. Turnbull, Plasma Phys. Controlled Fusion **36**, 1211 (1994).
[65]W. W. Heidbrink, E. J. Strait, M. S. Chu, and A. D. Turnbull, Phys. Rev. Lett. **71**, 855 (1993).
[66]W. W. Heidbrink, E. D. Fredrickson, T. K. Mau, C. C. Petty, R. I. Pinsker, M. Porkolab, and B. W. Rice, Nucl. Fusion **39**, 1369 (1999).
[67]M. Saigusa, H. Kimura, S. Moriyama, Y. Neyatani, T. Fujii, Y. Koide, T. Kondoh, M. Sato, M. Nemoto, Y. Kamada, and JT-60 Team, Plasma Phys. Controlled Fusion **37**, 295 (1995).
[68]M. Saigusa, H. Kimura, Y. Kusama, G. J. Kramer, T. Ozeki, S. Moriyama, T. Oikawa, Y. Neyetani, and T. Kondoh, Plasma Phys. Controlled Fusion **40**, 1647 (1998).
[69]G. J. Kramer, M. Iwase, Y. Kusama, A. Morioka, M. Nemoto, T. Nishitani, K. Shinohara, S. Takeji, K. Tobita, T. Ozeki, C. Z. Cheng, G.-Y. Fu, and R. Nazikian, Nucl. Fusion **40**, 1383 (2000).
[70]K. Tobita, Y. Kusama, K. Shinohara, T. Nishitani, H. Kimura, G. J. Kramer, M. Nemoto, T. Kondoh, T. Oikawa, A. Morioka, K. Hamamatsu, S. Wang, S. Takeji, M. Takechi, M. Ishikawa, K. Tani, M. Saigusa, and T. Ozeki, Fusion, Sci. Technol. **42**, 315 (2002).
[71]S. Ali-Arshad and D. J. Campbell, Plasma Phys. Controlled Fusion **37**, 715 (1995).
[72]A. Fasoli, D. Borba, G. Bosia, D. J. Campbell, J. A. Dobbing, C. Gormezano, J. Jacquinot, P. Lavanchy, J. B. Lister, P. Marmillod, J. M. Moret, A. Santagiustina, and S. Sharapov, Phys. Rev. Lett. **75**, 645 (1995).
[73]A. Fasoli, D. Borba, C. Gormezano, R. Heeter, A. Jaun, J. Jacquinot, W. Kerner, Q. King, J. B. Lister, S. Sharapov, D. Start, and L. Villard, Plasma Phys. Controlled Fusion **39**, B287 (1997).
[74]A. Fasoli, J. A. Dobbing, C. Gormezano, J. Jacquinot, J. B. Lister, S. E. Sharapov, and A. Sibley, Nucl. Fusion **36**, 258 (1996).
[75]A. Fasoli, J. B. Lister, S. E. Sharapov, S. Ali-Arshad, G. Bosia, D. Borba, D. J. Campbell, N. Deliyanakis, J. A. Dobbing, C. Gormezano, H. A. Holties, G. T. A. Huysmans, J. Jacquinot, A. Jaun, W. Kerner, P. Lavanchy, J. M. Moret, L. Porte, A. Santagiustina, and L. Villard, Nucl. Fusion **35**, 1485 (1995).
[76]A. Fasoli, B. N. Breizman, D. Borba, R. F. Heeter, M. S. Pekker, and S. E. Sharapov, Phys. Rev. Lett. **81**, 5564 (1998).
[77]W. W. Heidbrink, A. Fasoli, D. Borba, and A. Juan, Phys. Plasmas **4**, 3663 (1997).
[78]A. Fasoli, D. Testa, S. Sharapov, H. L. Berk, B. Breizman, A. Gondhalekar, R. F. Heeter, and M. Mantsinen, Plasma Phys. Controlled Fusion **44**, B159 (2002).
[79]D. Testa, A. Fasoli, A. Jaun, and JET-EFDA Contributors, Nucl. Fusion **43**, 724 (2003).
[80]W. W. Heidbrink, E. Fredrickson, N. N. Gorelenkov, A. W. Hyatt, G. Kramer, and Y. Luo, Plasma Phys. Controlled Fusion **45**, 983 (2003).
[81]E. D. Fredrickson, W. W. Heidbrink, C. Z. Cheng, N. N. Gorelenkov, E. Belova, A. W. Hyatt, G. J. Kramer, J. Manickam, J. Menard, R. Nazikian, T. L. Rhodes, and E. Ruskov, in *Proceedings of the 20th International Conference on Plasma Physics and Controlled Nuclear Fusion Research*, Vilamoura, Portugal, 2004 (International Atomic Energy Agency, Vienna, 2005), CD-ROM file EX/5-3.
[82]N. A. Crocker, W. A. Peebles, S. Kubota, E. D. Fredrickson, S. M. Kaye, B. P. LeBlanc, and J. E. Menard, Phys. Rev. Lett. **97**, 045002 (2006).
[83]A. Sykes, R. J. Akers, L. C. Appel, E. R. Arends, P. G. Carolan, N. J. Conway, G. F. Counsell, G. Cunningham, A. Dnestrovskij, Yu. N. Dnestrovskij, A. R. Field, S. J. Fielding, M. P. Gryaznevich, S. Korsholm, E. Laird, R. Martin, M. P. S. Nightingale, C. M. Roach, M. R. Tournianski, M. J. Walsh, C. D. Warrick, H. R. Wilson, S. You, MAST Team, and NBI Team, Nucl. Fusion **41**, 1423 (2001).
[84]M. P. Gryaznevich and S. E. Sharapov, Plasma Phys. Controlled Fusion **46**, S15 (2004).
[85]S. D. Pinches, H. L. Berk, M. P. Grayaznevich, S. E. Sharapov, and JET-EFDA Contributors, Plasma Phys. Controlled Fusion **46**, S47 (2004).
[86]S. E. Sharapov, B. Alper, F. Andersson, Yu. F. Baranov, H. L. Berk, L. Bertalot, D. Borba, C. Boswell, B. N. Breizman, R. Buttery, C. D. Challis, M. de Baar, L.-G. de Vries, A. Eriksson, R. Fasoli, V. Galvao. M. P. Goloborod'ko, R. J. Gryaznevich, N. C. Hastie, P. Hawkes, V. G. Helander, G. J. Kiptily, P. J. Kramer, J. Lomas, M. J. Mailloux, R. Mantsinen, F. Martin, M. F. Nabais, R. Nave, J.-M. Nazikian, M. S. Noterdaeme, S. D. Pekker, T. Pinches, S. V. Pinfold, P. Popovichev, D. Sandquist, D. Stork, A. Testa, I. Tuccillo, V. Voitsekhovich, N. P. Yavorskij, F. Young, F. Zonca, JET-EFDA Contributors, and MAST Team, Nucl. Fusion **45**, 1168 (2005).
[87]K. G. McClements, M. P. Gryaznevich, S. E. Sharapov, R. J. Akers, L. C. Appel, G. F. Counsel, C. M. Roach, and R. Majeski, Plasma Phys. Controlled Fusion **41**, 661 (1999).
[88]M. P. Gryaznevich and S. E. Sharapov, Nucl. Fusion **40**, 907 (2000).
[89]H. L. Gorelenkov, R. Berk, C. Z. Budny, G.-Y. Cheng, W. W. Fu, G. J. Heidbrink, D. Kramer, D. Meade, and R. Nazikian, Nucl. Fusion **43**, 594 (2003).
[90]K. L. Wong, Plasma Phys. Controlled Fusion **41**, R1 (1999).
[91]M. A. Van Zeeland, W. W. Heidbrink, R. Nazikian, M. E. Austin, C. Z. Cheng, M. S. Chu, N. N. Gorelenkov, C. T. Holcomb, A. W. Hyatt, G. J. Kramer, J. Lohr, G. R. McKee, C. C. Petty, R. Prater, W. M. Solomon, and D. A. Spong, Nucl. Fusion **49**, 065003 (2009).
[92]Y. Todo, K. Shinohara, M. Takechi, and M. Ishikawa, Phys. Plasmas **12**, 012503 (2005).
[93]Y. Todo, H. L. Berk, and B. N. Breizman, Phys. Plasmas **10**, 2888 (2003).
[94]ITER Physics Expert Group on Energetic Particles, Heating and Current Drive, Nucl. Fusion **39**, 2471 (1999).
[95]E. D. Fredrickson, N. N. Gorelenkov, R. E. Bell, J. E. Menard, A. L. Roquemore, S. Kubota, N. A. Crocker, and W. Peebles, Nucl. Fusion **46**, S926 (2006).
[96]M. Podestà, W. W. Heidbrink, D. Liu, E. Ruskov, R. E. Bell, D. S. Darrow, E. D. Fredrickson, N. N. Gorelenkov, G. J. Kramer, B. P. LeBlanc, S. S. Medley, A. L. Roquemore, N. A. Crocker, S. Kubota, and H. Yuh, Phys. Plasmas **16**, 056104 (2009).
[97]H. L. Berk, B. N. Breizman, and M. Pekker, Phys. Plasmas **2**, 3007 (1995).
[98]C. Z. Cheng, Phys. Rep. **211**, 1 (1992).
[99]N. N. Gorelenkov, C. Z. Cheng, and G. Y. Fu, Phys. Plasmas **6**, 2802 (1999).
[100]R. B. White and M. S. Chance, Phys. Fluids **27**, 2455 (1984).
[101]F. M. Levinton and H. Yuh, Rev. Sci. Instrum. **79**, 10F522 (2008).
[102]D. W. Johnson, N. Bretz, B. LeBlanc, R. Palladino, D. Long, and R. Parsells, Rev. Sci. Instrum. **70**, 776 (1999).
[103]R. E. Bell, B. P. LeBlanc, C. Bourdelle, D. R. Ernst, E. D. Fredrickson, D. A. Gates, J. C. Hosea, D. W. Johnson, S. M. Kaye, R. Maingi, S. Medley, J. E. Menard, D. Mueller, M. Peng, M. Ono, F. Paoletti, S. A. Sabbagh, D. Stutman, D. W. Swain, E. J. Synakowski, and J. R. Wilson, in *Proceedings of the 28th EPS Conference on Controlled Fusion and Plasma Physics*, Funchal, 2001 (The European Physical Society, Geneva, 2001), Vol. 25A, p. 1021.
[104]D. Stutman, M. Finkenthal, V. Soukhanovskii, M. J. May, H. W. Moos, and R. Kaita, Rev. Sci. Instrum. **70**, 572 (1999).
[105]S. S. Medley, R. E. Bell, M. P. Petrov, A. L. Roquemore, and E. V. Suvorkin, Rev. Sci. Instrum. **74**, 1896 (2003).
[106]D. Liu, W. W. Heidbrink, D. S. Darrow, A. L. Roquemore, S. S. Medley, and K. Shinohara, Rev. Sci. Instrum. **77**, 10F113 (2006).
[107]D. S. Darrow, Rev. Sci. Instrum. **79**, 023502 (2008).
[108]R. V. Budny, Nucl. Fusion **34**, 1247 (1994).
[109]H. Kimura, Y. Kusama, M. Saigusa, G. J. Kramer, K. Tobita, M. Nemoto, T. Kondoh, T. Nishitani, O. da Costa, T. Ozeki, T. Oikawa, S. Moriyama, A. Morioka, G. Y. Fu, C. Z. Cheng, and V. I. Afanas'ev, Nucl. Fusion **38**, 1303 (1998).
[110]S. E. Sharapov, D. Testa, B. Alper, D. N. Borba, A. Fasoli, N. C. Hawkes, R. F. Heeter, M. J. Mantsinen, M. von Hellermann, Phys. Lett. A **289**, 127 (2001).
[111]H. L. Berk, D. N. Borba, B. N. Breizman, S. D. Pinches, and S. E. Sharapov, Phys. Rev. Lett. **87**, 185002 (2001).
[112]S. E. Sharapov, B. Alper, H. L. Berk, D. N. Borba, B. N. Breizman, D. C. D. Challis, A. Fasoli, N. C. Hawkes, T. C. Hender, J. Mailloux, S. D. Pinches, and D. Testa, Phys. Plasmas **9**, 2027 (2002).
[113]B. N. Breizman, H. L. Berk, M. S. Pekker, S. D. Pinches, and S. E. Sharapov, Phys. Plasmas **10**, 3649 (2003).
[114]S. E. Sharapov, B. Alper, J. Fessey, N. C. Hawkes, N. P. Young, R. Nazikian, G. J. Kramer, D. N. Borba, S. Hacquin, E. De La Luna, S. D. Pinches, J. Rapp, D. Testa, and JET-EFDA Contributors, Phys. Rev. Lett. **93**, 165001 (2004).
[115]J. A. Snipes, N. Basse, C. Boswell, E. Edlund, A. Fasoli, N. N. Gorelenkov, and R. S. Granetz, L. Lin, Y. Lin, R. Parker, M. Porkolab, J. Sears, S. Sharapov, V. Tang, and S. Wukitch, Phys. Plasmas **12**, 056102 (2005).
[116]B. N. Breizman and M. S. Pekker, Phys. Plasmas **12**, 112506 (2005).
[117]E. D. Fredrickson, N. A. Crocker, N. N. Gorelenkov, W. W. Heidbrink, S. Kubota, F. M. Levinton, H. Yuh, J. E. Menard, and R. E. Bell, Phys. Plasmas **14**, 102510 (2007).

[118]N. A. Crocker, E. D. Fredrickson, N. N. Gorelenkov, G. J. Kramer, D. S. Darrow, W. W. Heidbrink, S. Kubota, F. M. Levinton, H. Yuh, J. E. Menard, B. P. LeBlanc, and R. E. Bell, Phys. Plasmas **15**, 102502 (2008).

[119]G. J. Kramer, R. Nazikian, B. Alper, M. de Baar, H. L. Berk, G.-Y. Fu, N. N. Gorelenkov, G. McKee, S. D. Pinches, T. L. Rhodes, S. E. Sharapov, W. M. Solomon, and M. A. van Zeeland, Phys. Plasmas **13**, 056104 (2006).